




LAMTOR1 inhibition of TRPML1-dependent lysosomal calcium release regulates dendritic lysosome trafficking and hippocampal neuronal function

Jiandong Sun^{1,*} , Yan Liu², Xiaoning Hao¹, Weiju Lin², Wenyue Su², Emerald Chiang² , Michel Baudry² & Xiaoning Bi^{1,**} 

Abstract

Lysosomes function not only as degradatory compartments but also as dynamic intracellular calcium ion stores. The transient receptor potential mucolipin 1 (TRPML1) channel mediates lysosomal Ca²⁺ release, thereby participating in multiple cellular functions. The pentameric Ragulator complex, which plays a critical role in the activation of mTORC1, is also involved in lysosomal trafficking and is anchored to lysosomes through its LAMTOR1 subunit. Here, we report that the Ragulator restricts lysosomal trafficking in dendrites of hippocampal neurons via LAMTOR1-mediated tonic inhibition of TRPML1 activity, independently of mTORC1. LAMTOR1 directly interacts with TRPML1 through its N-terminal domain. Eliminating this inhibition in hippocampal neurons by LAMTOR1 deletion or by disrupting LAMTOR1-TRPML1 binding increases TRPML1-mediated Ca²⁺ release and facilitates dendritic lysosomal trafficking powered by dynein. LAMTOR1 deletion in the hippocampal CA1 region of adult mice results in alterations in synaptic plasticity, and in impaired object-recognition memory and contextual fear conditioning, due to TRPML1 activation. Mechanistically, changes in synaptic plasticity are associated with increased GluA1 dephosphorylation by calcineurin and lysosomal degradation. Thus, LAMTOR1-mediated inhibition of TRPML1 is critical for regulating dendritic lysosomal motility, synaptic plasticity, and learning.

Keywords calcineurin; calcium; dynein; LTD; LTP

Subject Categories Neuroscience; Organelles

DOI 10.15252/embj.2021108119 | Received 24 February 2021 | Revised 12 December 2021 | Accepted 21 December 2021 | Published online 31 January 2022

The EMBO Journal (2022) 41: e108119

Introduction

The view that the lysosome is merely a degradation machinery has been challenged by recent studies demonstrating other critical roles for this organelle. Thus, lysosomes provide platforms for and coordinate energy sensing and regulation of various cell signaling pathways, for example, signaling via the mechanistic target of rapamycin complex 1 (mTORC1) (Nada *et al*, 2009; Sancak *et al*, 2010; Zhang *et al*, 2014). Emerging evidence also indicates that the late endosomal-lysosomal system (referred to as lysosomes for simplicity hereafter) serves as an important intracellular Ca²⁺ store with multiple channels/transporters, which regulate Ca²⁺ release and refilling (Morgan *et al*, 2011; Xu & Ren, 2015). Lysosomal Ca²⁺ release is required for diverse physiological functions, including lysosomal motility (Li *et al*, 2016) and exocytosis (Medina *et al*, 2011; Samie *et al*, 2013; Park *et al*, 2016), phagocytosis (Davis *et al*, 2020), and autophagy (Medina *et al*, 2015). It has recently been shown that neuronal activity recruits lysosomes into dendritic spines (Goo *et al*, 2017), and triggers lysosomal Ca²⁺ release, which contributes to spine plasticity in hippocampal pyramidal neurons (Padamsey *et al*, 2017). However, research on lysosomal Ca²⁺ release-mediated signaling in neurons is still in its infancy and its regulation is largely unknown.

The transient receptor potential mucolipin 1 (TRPML1) channel mediates lysosomal Ca²⁺ release, and mutations of this channel lead to the lysosomal storage disorder, mucopolipidosis type IV (MLIV), which is characterized by severe intellectual disability, motor and speech deficits, and progressive visual impairment (Misko *et al*, 2021). TRPML1 activity is regulated by pH (Raychowdhury *et al*, 2004), and its response to its endogenous agonist, PI(3,5)P₂, differs in lysosomes localized in perinuclear vs. peripheral areas of the cell (Dong *et al*, 2010; Zhang *et al*, 2012). In non-neuronal cells, PI(3,5)P₂-induced TRPML1 activation promotes Ca²⁺-dependent centripetal lysosomal trafficking in an ALG-2-dynein-dependent manner (Li *et al*, 2016). In hippocampal neurons, dynein drives cargo transport

1 College of Osteopathic Medicine of the Pacific, Western University of Health Sciences, Pomona, CA, USA

2 Graduate College of Biomedical Sciences, Western University of Health Sciences, Pomona, CA, USA

*Corresponding author. Tel: +1 909 469 5471; E-mail: sjdpillar@gmail.com

**Corresponding author. Tel: +1 909 469 5487; E-mail: xbi@westernu.edu

from soma into proximal dendrites, bidirectionally steered by mixed polarized microtubules (Kapitein *et al*, 2010). These findings have suggested that the TRPML1-dynein machinery could play an important role in dendritic lysosomal trafficking.

The lysosome-localized Ragulator complex interacts with the BLOC-1-related complex (BORC), thereby regulating lysosome trafficking in nonneuronal cells (Filipek *et al*, 2017; Pu *et al*, 2017). The Ragulator complex consists of LAMTOR1 (aka p18), LAMTOR2 (p14), LAMTOR3 (MP1), LAMTOR4 (C7orf59), and LAMTOR5 (HBXIP), and plays a critical role in lysosomal recruiting and activation of mTORC1 (Nada *et al*, 2009; Sancak *et al*, 2010; Bar-Peled *et al*, 2012). BORC promotes kinesin-dependent lysosome centrifugal trafficking, which is inhibited by the Ragulator, independently of mTOR. In neurons, the BORC-kinesin mechanism specifically drives lysosome transport into axons but not dendrites (Farias *et al*, 2017). Very little is known regarding the roles of the Ragulator in lysosome trafficking in dendrites. The present study investigated the mechanisms underlying Ragulator-mediated regulation of lysosomal trafficking in dendrites of hippocampal neurons and their functional implications. The results indicate that LAMTOR1 regulates lysosomal trafficking and GluA1 dephosphorylation and degradation by tonically inhibiting lysosomal Ca^{2+} release through direct TRPML1 interaction and independently of mTORC1. Moreover, this mechanism plays a critical role in synaptic plasticity and learning and memory.

Results

LAMTOR1 regulates lysosomal trafficking in dendrites of hippocampal neurons

To examine lysosomal trafficking in neurons, cultured hippocampal neurons were incubated with LysoTracker, which preferentially labels lysosomal compartments (Chazotte, 2011). LysoTracker-labeled puncta were distributed throughout dendritic arbors and in some dendritic spines (Figs 1A and EV1A). LysoTracker fluorescence was mostly abolished by incubation with glycyl-L-phenylalanine 2-naphthylamide (GPN; 40 μ M, 5–10 min), a

compound widely used to produce osmotic lysis of lysosomal compartments (Padamsey *et al*, 2017) (Fig 1A).

To investigate whether the Ragulator, and in particular LAMTOR1, could regulate lysosomal trafficking in dendrites, we used AAV-mediated shRNA knock-down (KD) of LAMTOR1. Hippocampal neurons were transduced at day 7 *in vitro* (DIV7) with LAMTOR1 shRNA or scrambled shRNA and were tested 14 days later (the same protocol was used for the following experiments unless otherwise indicated). Live-cell imaging of lysosomes loaded with LysoTracker (Movies EV1–EV3) in scrambled shRNA-infected neurons showed that the percentage of mobile lysosomes (assessed by kymographs, Fig 1B, top panels and Appendix Fig S1A and B) in dendritic shafts was $42.4 \pm 2.3\%$ with $17.5 \pm 1.3\%$ and $24.9 \pm 1.8\%$ moving in anterograde and retrograde directions, respectively (Fig 1C). LAMTOR1 KD significantly increased the overall percentage of mobile lysosomes to $75.4 \pm 1.4\%$, with increased trafficking in both directions (Fig 1C), even though the total number of lysosomes was also increased (Appendix Fig S1C). Co-expressing shRNA-resistant LAMTOR1 in neurons (Fig EV1B and C) prevented LAMTOR1 shRNA-induced increase in lysosomal trafficking, confirming that the effect was due to LAMTOR1 KD (Fig 1B and C). Further analysis of velocities and traveled distances of mobile lysosomes based on their moving tracks (Fig 1B, bottom panels) showed that LAMTOR1 KD significantly and selectively increased the speed and travel distance of those with higher fluorescent intensity (Fig 1D and E), which correlates with higher acidity (Chakraborty *et al*, 2017; Hata *et al*, 2018). These effects were reversed by co-expression with shRNA-resistant LAMTOR1 (Figs 1D and E and EV1D–F).

We next analyzed the directional movement of lysosomes using fluorescence recovery after photobleaching (FRAP). In scrambled shRNA-infected neurons, equal numbers of lysosomes traveled retrogradely or anterogradely (Fig 1F and G). LAMTOR1 KD resulted in a significant increase in both anterograde and retrograde transport of lysosomes, and this increase was reversed by co-expression of shRNA-resistant LAMTOR1 (Fig 1F and G).

To analyze lysosome-mediated degradation, we incubated neurons with Magic Red cathepsin B fluorogenic substrates, which become fluorescent upon cathepsin B-mediated cleavage

Figure 1. LAMTOR1 regulates lysosomal trafficking in dendrites of hippocampal neurons.

- A Disruption of lysosomes with GPN abolished LysoTracker staining (red) in GFP-expressing hippocampal neurons. Scale bar, 20 μ m.
- B Upper panels: Kymographs of LysoTracker-labeled lysosomes in the proximal dendrites of neurons infected with scrambled shRNA (shSc), LAMTOR1 shRNA (shLAMTOR1), or LAMTOR1 shRNA and RNAi-resistant LAMTOR1 (rLAMTOR1). Stationary, anterograde, and retrograde traces generated using the KymoGraphClear plugin for ImageJ were coded blue, red, and green, respectively. Lower panels: Tracks of mobile lysosomes. Scale bar, 5 μ m.
- C Quantitative analysis of lysosomal movement from kymographs. Results were expressed as percent of total lysosomes ($N = 44, 49,$ and 16 neurons for shSc, shLAMTOR1, and shLAMTOR1+rLAMTOR1 respectively from 3 to 10 independent experiments).
- D, E Quantification of track speed (D) and displacement length (E) of lysosomes with low (0–1,000 arbitrary unit) and high ($> 1,000$) intensity of LysoTracker (dashed line, median; thin dashed line, quartiles; same length dendrites for each group from 3 independent experiments were analyzed).
- F, G FRAP analysis of dendritic lysosome movement. (F) Representative images of neurons at 0 and 4 min after photobleaching. Photobleached regions are indicated by the cyan and red lines, and lysosomes traveling anterogradely (crossing cyan line first) or retrogradely (crossing red line first) are labeled cyan and red, respectively. (G) Quantitative analysis for (F) ($N = 7, 7,$ and 9 neurons for shSc, shLAMTOR1, and shLAMTOR1+rLAMTOR1, respectively, from 3 independent experiments).
- H Left: Kymographs of Magic Red cathepsin B substrate-labeled degradative lysosomes in the proximal dendrites of neurons infected with shSc and shLAMTOR1. Scale bar, 5 μ m. Right: Quantitative analysis of vesicular movement from kymographs ($N = 16$ neurons from 3 independent experiments).

Data information: Data with error bars are represented as means \pm SEM. Statistical significance was assessed by two-way ANOVA with Tukey's (C), Dunnett's post-test (D, E, G), or Mann–Whitney U test (H). * $P < 0.05$, ** $P < 0.01$, *** $P < 0.001$, as compared to shSc; # $P < 0.05$, ### $P < 0.001$, as compared to shLAMTOR1 (C–E, G); n.s., not significant. See also Fig EV1 and Appendix Fig S1.

Source data are available online for this figure.

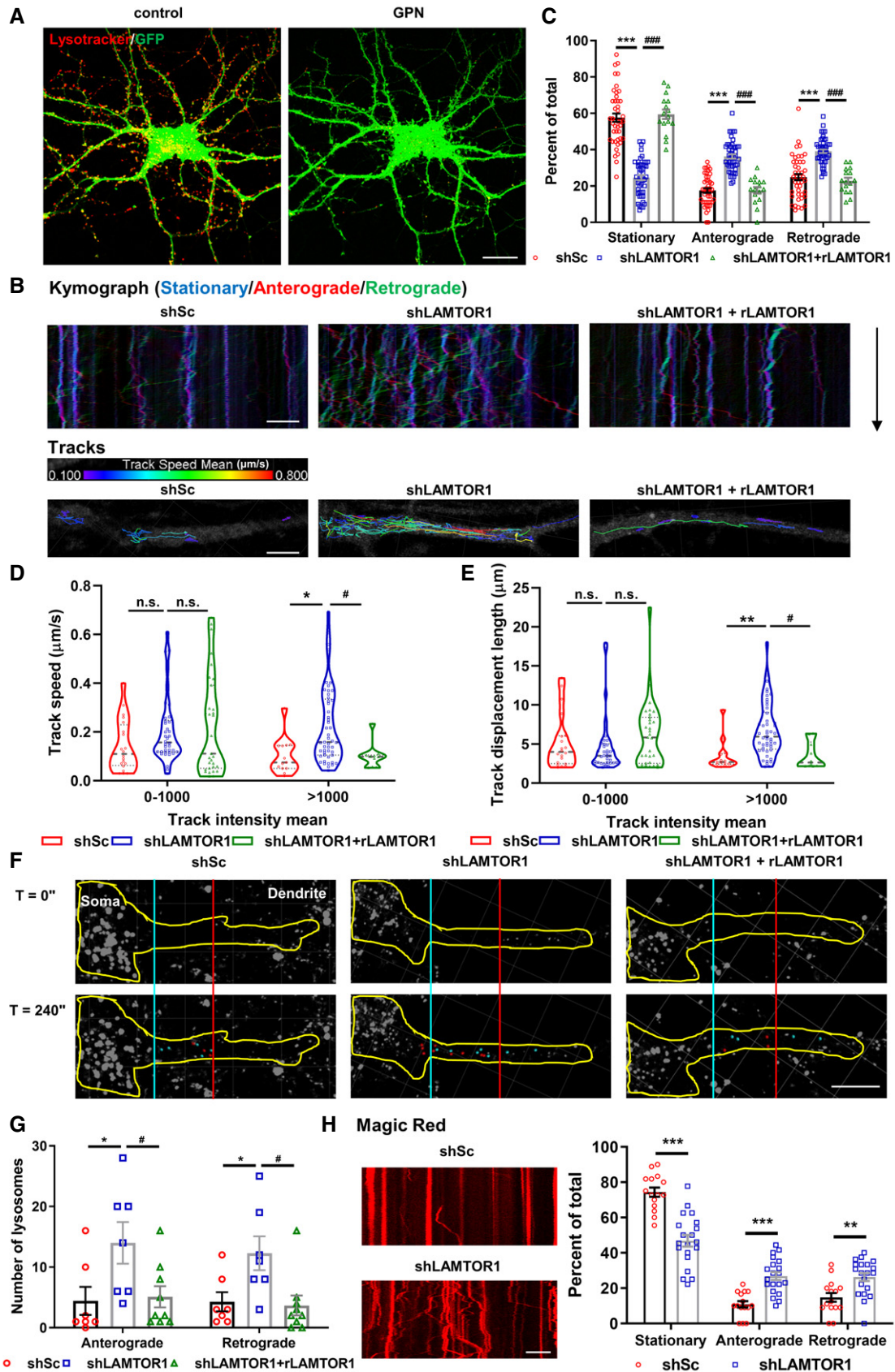


Figure 1.

(Farfel-Becker *et al*, 2019). Live imaging revealed the presence of lysosomes containing active cathepsin B along dendrites (Movies EV4–EV5). In the dendritic shafts of scrambled shRNA-infected neurons, the majority of degradative lysosomes were stationary with only $10.9 \pm 1.8\%$ and $14.8 \pm 2.5\%$ moving in anterograde and retrograde directions, respectively (Fig 1H). LAMTOR1 KD significantly increased the overall percentage of mobile degradative lysosomes from $25.7 \pm 2.6\%$ to $53.2 \pm 3.3\%$, with increased trafficking in both directions (Fig 1H).

To confirm the effect of LAMTOR1 KD on lysosome motility, we used LAMP1-YFP (transfected at DIV7) to label lysosomes in cultured hippocampal neurons transfected with Accell control or LAMTOR1 siRNA (at DIV4), and lysosomal trafficking was recorded at DIV8. Trafficking of LAMP1-YFP-labeled lysosomes was also significantly enhanced by LAMTOR1 KD (Fig EV1G).

LAMTOR1 regulation of dendritic lysosomal trafficking depends on the integrity of the Ragulator but not on mTORC1

We next determined whether knocking down other Ragulator members could also change lysosomal trafficking in cultured hippocampal neurons. LAMTOR2 KD also increased lysosomal mobility, similarly to LAMTOR1 KD (Fig 2A and B). As previously reported (Scheffler *et al*, 2014), LAMTOR2 KD resulted in down-regulation of other members of the Ragulator, that is, LAMTOR4 and LAMTOR1 (Appendix Fig S2A and D). We then tested whether the ability of the Ragulator to control lysosomal trafficking depended on mTORC1. AAV-mediated shRNA KD of Raptor, an essential component of mTORC1, reduced lysosomal mTOR localization (Appendix Fig S2B and C), as previously reported in HeLa cells (Pu *et al*, 2017). However, Raptor KD did not alter dendritic lysosomal mobility in neurons (Fig 2A and B), although both LAMTOR1 KD and Raptor KD reduced the phosphorylation of S6K1 and S6, which are downstream mTORC1 signaling proteins (Hay & Sonenberg, 2004). LAMTOR2 KD increased mTORC1 signaling (Appendix Fig S2D), an effect similar to that reported in LAMTOR2-deficient dendritic cells (Scheffler *et al*, 2014). FRAP results further confirmed that Raptor KD had no effect on either anterograde or retrograde transport of lysosomes (Fig 2C and D). Furthermore, treatment with an inhibitor of mTOR, Torin 1 (250 nM), for 2.5 h had no effect on dendritic lysosomal trafficking (Appendix Fig S2E and F). These results indicate that lysosomal trafficking in dendrites of hippocampal neurons is regulated by the Ragulator but not by mTORC1.

To investigate whether LAMTOR1 KD could affect other endocytic organelle trafficking in dendrites, we incubated cultured hippocampal neurons with Alexa 594-conjugated transferrin, which labels early and recycling endosomes (Mayle *et al*, 2012). Live-cell imaging showed that the movement of transferrin-labeled endosomes was comparable in scrambled and LAMTOR1 shRNA-infected neurons (Fig 2E and F), supporting a specific effect of LAMTOR KD on lysosomal trafficking.

LAMTOR1 KD-induced changes in lysosomal trafficking require TRPML1-mediated Ca^{2+} release and dynein activation

We next determined the potential mechanism underlying LAMTOR1 KD-induced increase in lysosomal mobility. In cultured rat hippocampal neurons, BORC has been shown to play an important role in regulating lysosomal trafficking; it specifically drives lysosomes into axons but not dendrites (Farias *et al*, 2017). We examined the effect of Accell siRNA-mediated KD of lyspersin, which has been shown to be the linker between BORC and Ragulator (Filipek *et al*, 2017; Pu *et al*, 2017), on dendritic lysosomal trafficking in control and LAMTOR1 KD neurons. The results showed that lyspersin KD had no obvious effects on lysosome trafficking in dendrites of either control or LAMTOR1 KD neurons (Fig 3A and Appendix Fig S3), suggesting that the BORC complex is unlikely to play a major role in LAMTOR1-mediated regulation of lysosomal motility in neuronal dendrites.

TRPML1-mediated Ca^{2+} release has been shown to regulate retrograde lysosomal transport through ALG-2 and the recruiting of the motor protein dynein (Li *et al*, 2016). To determine whether TRPML1-mediated Ca^{2+} release could contribute to LAMTOR1 KD-induced changes in lysosomal trafficking, we used both pharmacological and genetic strategies (Fig 3B). Treatment with an inhibitor of TRPML1, ML-SI1 (20 μM), for 2 h blocked LAMTOR1 KD-induced changes in lysosomal trafficking (Fig 3C and Appendix Fig S3). Similarly, Accell siRNA-mediated TRPML1 KD reversed LAMTOR1 KD-induced changes (Fig 3D and Appendix Fig S3). On the other hand, direct activation of TRPML1 with ML-SA1 (20 μM , 1.5 h) in scrambled shRNA-treated neurons increased both anterograde and retrograde lysosome trafficking (Fig 3E and Appendix Fig S3). ML-SA1 treatment did not further increase lysosomal trafficking in LAMTOR1 KD neurons (Fig 3E and Appendix Fig S3).

To determine whether dynein was involved, we treated neurons with the dynein inhibitor ciliobrevin D (20 μM , 1.5 h); the low

Figure 2. LAMTOR1 regulates dendritic lysosome trafficking independently of mTORC1.

- A Representative kymographs of LysoTracker-labeled lysosomes in proximal dendrites of hippocampal neurons infected with scrambled shRNA (shSc), LAMTOR2 shRNA (shLAMTOR2), or Raptor shRNA (shRaptor). Scale bar, 5 μm .
- B Quantitative analysis of lysosomal movement from kymographs ($N = 44, 24,$ and 19 neurons for shSc, shLAMTOR2, and shRaptor, respectively, from 3 to 10 independent experiments).
- C, D FRAP analysis of dendritic lysosomal movement in Raptor KD neurons. (C) Representative images of a neuron at 0 and 4 min after photobleaching. (D) Quantification of the lysosomes in (C) undergoing retrograde (red) or anterograde (cyan) transport ($N = 7$ and 8 neurons for shSc and shRaptor, respectively, from 3 independent experiments).
- E LAMTOR1 KD did not affect trafficking of vesicles labeled with Alexa 594-conjugated transferrin (red, Tf 594) in dendrites. Shown are dendritic segments (upper) and kymographs (lower). Scale bar, 5 μm .
- F Quantitative analysis of vesicular movement from kymographs ($N = 10$ neurons from 3 independent experiments).

Data information: Data with error bars are represented as means \pm SEM. Statistical significance was assessed by two-way ANOVA with Sidak's post-test (B) and Mann–Whitney U test (D, F). *** $P < 0.001$ as compared to shSc; n.s., not significant. See also Appendix Fig S2.

Source data are available online for this figure.

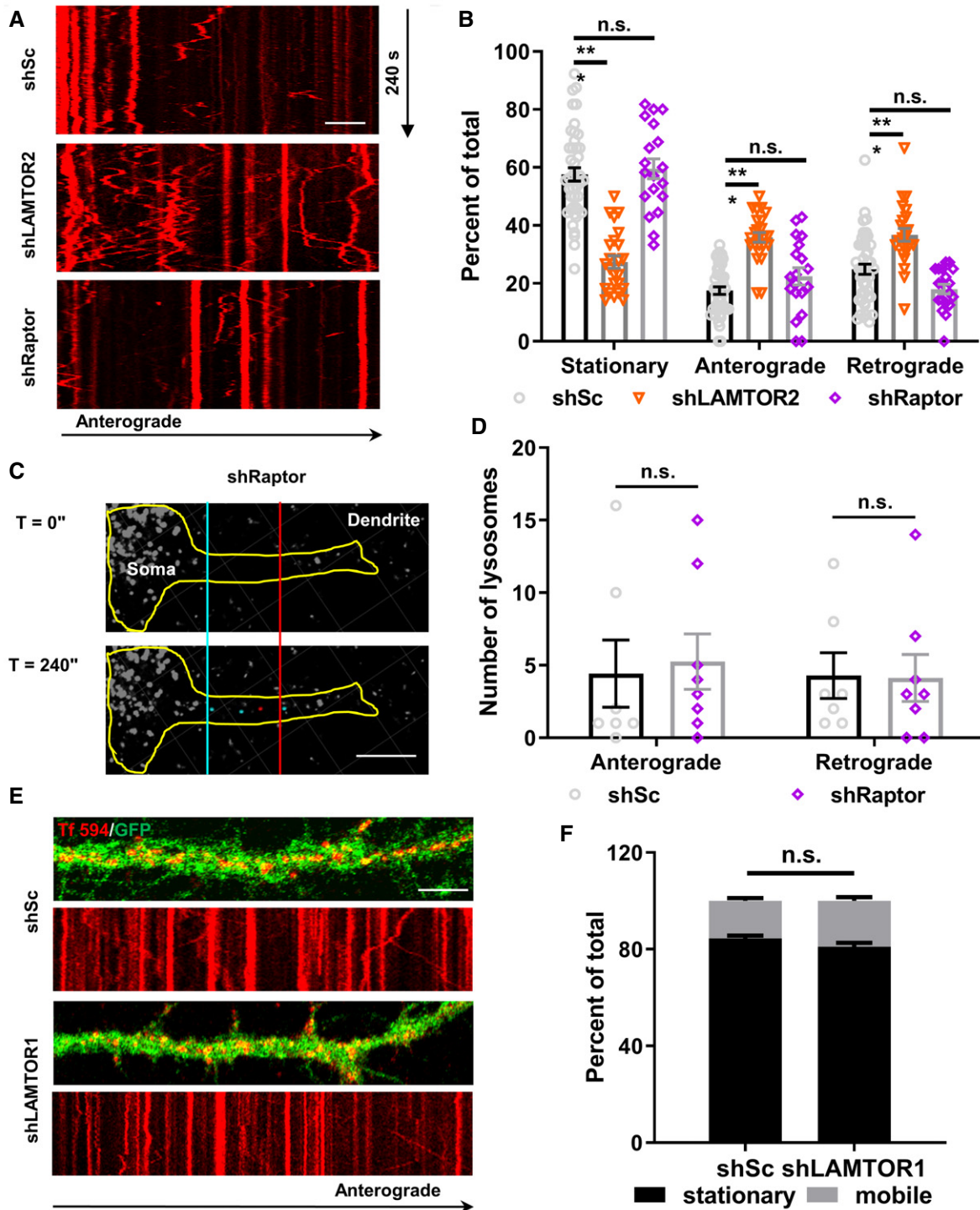


Figure 2.

concentration of ciliobrevin D (Firestone *et al*, 2012) was chosen to selectively disrupt dynein-dependent cargo trafficking without affecting microtubule organization in dendrites as previously reported (Ayloo *et al*, 2017). Inhibition of dynein in LAMTOR1 KD neurons reduced both the retrograde and anterograde movement of lysosomes (Fig 3F and Appendix Fig S3), suggesting that dynein

participates in bidirectional lysosomal trafficking in dendrites. This conclusion is consistent with the observation that the percentage of inward and outward oriented microtubules in dendritic shafts is similar (Baas *et al*, 1988; Tas *et al*, 2017). Ciliobrevin D treatment had no significant effect in scrambled shRNA-transfected neurons (Fig 3F and Appendix Fig S3). These data support our proposed

model (Fig 3B) in which TRPML1-mediated Ca²⁺ release plays an important role in dynein-mediated lysosomal trafficking in dendrites and the activity of TRPML1 is tonically and negatively regulated by LAMTOR1.

LAMTOR1 directly interacts with TRPML1 and regulates its function

To understand how LAMTOR1 could regulate the activity of TRPML1, we analyzed interactions between LAMTOR1 and TRPML1

by first performing co-immunoprecipitation (co-IP) experiments in HeLa cells transfected with TRPML1-YFP and LAMTOR1-Flag. Structural studies of the Ragulator have revealed that, while the central region of LAMTOR1 wraps around two roadblock heterodimers, LAMTOR2-LAMTOR3 and LAMTOR4-LAMTOR5, its N- and C-terminal regions are disordered and more flexible (de Araujo et al, 2017; Yonehara et al, 2017). We therefore targeted these two regions for potential interaction sites with TRPML1, and prepared constructs with deletions of either the N- (residues 20 to 60) or C-terminal (residues 144 to 161) domains of LAMTOR1 (Fig 4A). Prominent

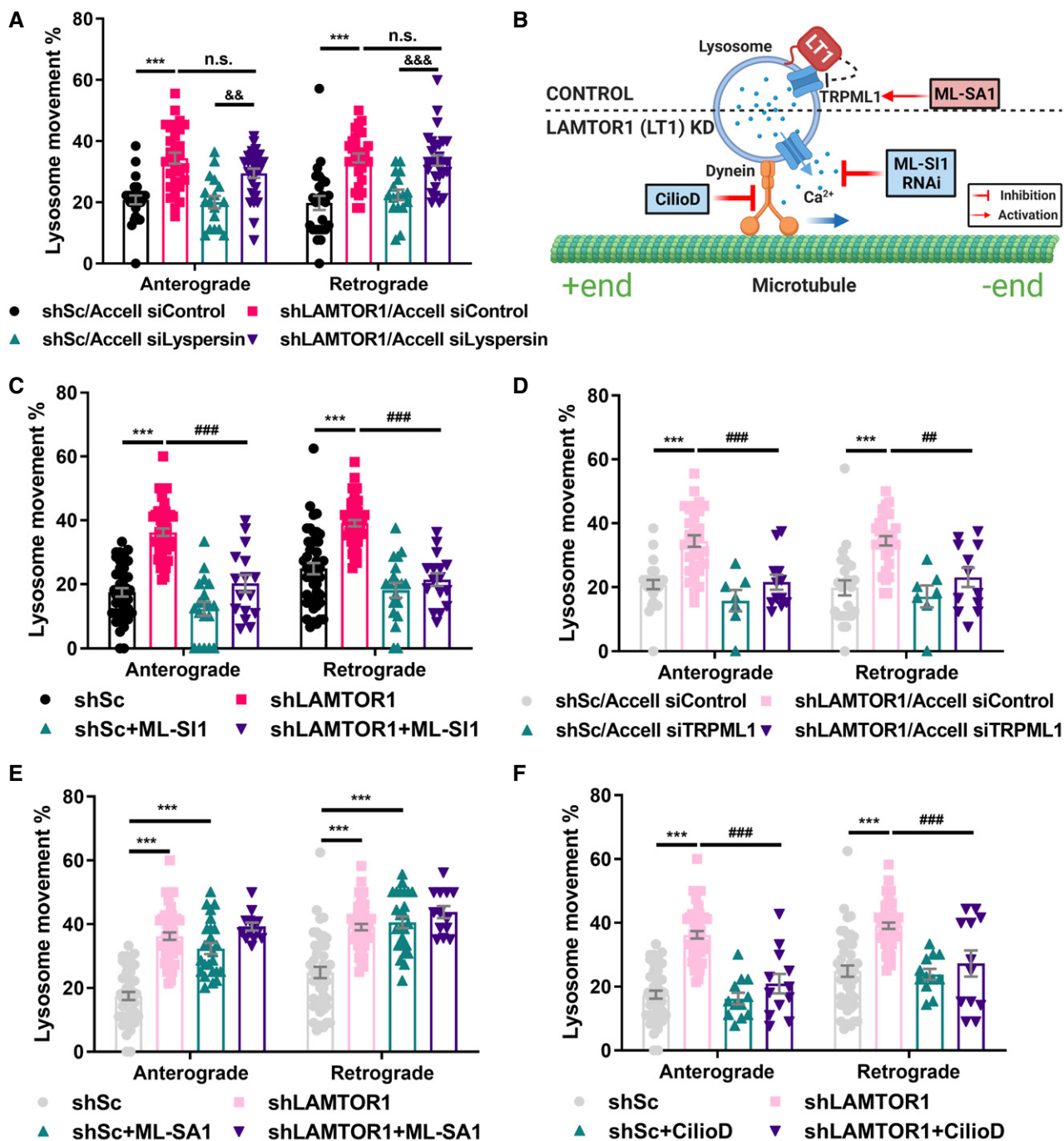


Figure 3.

Figure 3. LAMTOR1 KD-induced changes in lysosomal trafficking require TRPML1-mediated Ca²⁺ release and dynein activation.

- A Quantification of the percent of lysosomes moving in the anterograde or retrograde direction in neurons infected with AAV expressing either LAMTOR1 shRNA (shLAMTOR1) or scrambled shRNA (shSc) and Accell lysipersin siRNA or control siRNA. Neurons were imaged with LysoTracker to visualize lysosomal trafficking in dendrites. $N = 17\text{--}31$ neurons from 3 to 6 independent experiments.
- B Targets of pharmacological reagents and genetic manipulation used in this study. Blue text box, TRPML1 inhibition including TRPML1 inhibitor ML-S11, TRPML1 siRNA, and dynein inhibitor ciliobrevin D (CilioD); red text box, TRPML1 activation induced by TRPML1 activator ML-SA1. Dash line separates the lysosome into lysosomes under control and LAMTOR1 (LT1) KD conditions.
- C–F Quantification of the percent of lysosomes moving in the anterograde or retrograde direction. (C, E, F) Cultured hippocampal neurons were infected with AAV expressing either shLAMTOR1 or shSc; they were treated with vehicle control or ML-S11 (20 μM , C, $n = 16\text{--}49$ neurons from 3 to 10 independent experiments), or ML-SA1 (20 μM , E, $n = 13\text{--}49$ neurons from 3 to 10 independent experiments), or CilioD (20 μM , F, $n = 12\text{--}49$ neurons from 3 to 10 independent experiments), and imaged with LysoTracker to visualize lysosomal trafficking in dendrites. Note that the data of shSc and shLAMTOR1 in (C, E, and F) are the same as shown in Fig 1C. (D) Neurons were infected with shLAMTOR1 or shSc AAV and Accell TRPML1 siRNA or control siRNA; they were imaged as described above. $N = 7\text{--}31$ neurons from 3 to 6 independent experiments. Note that the data of shSc/Accell siControl and shLAMTOR1/Accell siControl in (D) are the same as shown in (A).

Data information: Data with error bars are represented as means \pm SEM. *** $P < 0.001$ compared with shSc or shSc/Accell siControl; ** $P < 0.01$, **** $P < 0.001$ compared with shLAMTOR1 or shLAMTOR1/Accell siControl; && $P < 0.01$, &&& $P < 0.001$ compared with shSc/Accell siLysipersin; n.s., not significant; two-way ANOVA with Tukey's post-test. See also Appendix Fig S3.

Source data are available online for this figure.

Flag-immunopositive bands were clearly present in anti-GFP (which recognizes YFP) pull-down products (Fig 4B; see Appendix Fig S4A for negative control). Similarly, GFP-immunopositive proteins were clearly pulled down by an anti-Flag antibody (Fig 4C; see Appendix Fig S4B for negative control). Co-IP results also showed that deletion of the N- but not the C-terminal domain significantly reduced LAMTOR1–TRPML1 interactions (Fig 4B and C and F). We next prepared two constructs with smaller deletions of the N-terminal (residues 20–31 or 42–60) domain (Fig 4A). Deletion of residues 20–31 but not residues 42–60 significantly decreased LAMTOR1–TRPML1 interactions (Fig 4D and F). We also engineered LAMTOR1 proteins with K20 and K31 to arginine substitution (K20R and K31R, Fig 4A), two potential ubiquitination sites (Wagner *et al*, 2011), and protein ubiquitination has been reported to be involved in endosomal trafficking (Jongsma *et al*, 2016). Co-IP results indicated that both K20R and K31R mutations significantly reduced LAMTOR1–TRPML1 interactions, with K31R having the largest effect (Fig 4E and F). Immunostaining analysis confirmed that these mutations did not affect LAMTOR1 lysosomal localization or colocalization with TRPML1 (Fig EV2A–D). In addition, we performed co-IP of TRPML1 and LAMTOR1 in starved HeLa cells. The result showed that starvation did not affect the LAMTOR1–TRPML1 interaction (Fig 4E and F). Using the Wes capillary electrophoresis protein detection system, we verified the interaction between endogenous LAMTOR1 and TRPML1 in mouse hippocampal tissues by co-IP (Fig 5A; validation of the TRPML1 antibody is shown in Appendix Fig S5A and B). Since residues 20–31 of LAMTOR1 are important for its interaction with TRPML1, we designed a peptide containing this sequence with the TAT peptide added to its N-terminal end (TAT-2031) to allow for its efficient delivery across cell membranes or the blood-brain barrier. We first tested whether this peptide could disrupt the interaction between LAMTOR1 and TRPML1 *in vivo*. Mice were injected with either control TAT or TAT-2031 (i.p., 50 mg/kg), and hippocampi were collected 2 h later. Co-IP experiments showed that LAMTOR1–TRPML1 interaction was significantly reduced in TAT-2031-treated mice, as compared to TAT-treated mice (Fig 5A and B). Furthermore, intact-cell cross-linking of fresh brain tissues using the chemical cross-linker dithiobis-(succinimidyl propionate) (DSP, see methods in Appendix for details) combined with co-IP experiments

confirmed the results (Appendix Fig S5C and D). We also performed a proximity ligation assay (PLA), which is an unbiased method to detect protein–protein interactions in hippocampal slices. A clear interaction between LAMTOR1 and TRPML1 was observed (Fig 5C), but not when the primary antibody was omitted (negative controls, Appendix Fig S5E). Of note, there was no interaction detected between LAMTOR4 and TRPML1 (Appendix Fig S5E). Consistent with the co-IP results, TAT-2031 treatment significantly reduced the interaction between LAMTOR1 and TRPML1 (Fig 5C and D). However, TAT-2031 did not affect the interaction between LAMTOR1 and other members of the Ragulator, nor did it affect mTOR activation, as assessed by phosphorylation of S6K1 and S6 (Fig EV2E and F). Finally, treatment with TAT-2031 (10 μM , 2 h) increased lysosomal mobility in neurons transfected with scrambled shRNA but not with LAMTOR1 shRNA (Fig 5E and Appendix Fig S3). Collectively, these results show that LAMTOR1 through its N-terminal (20–31) directly interacts with and inhibits TRPML1, thereby regulating lysosomal trafficking in dendrites.

To better assess the regulation of LAMTOR1 on TRPML1-mediated Ca²⁺ release, we genetically engineered a single-wavelength Ca²⁺ indicator (Chen *et al*, 2013), by attaching GCaMP6m to the cytoplasmic carboxyl-terminus of TRPML1 (Fig 6A). When transfected into HeLa cells, TRPML1-GCaMP6m was mainly localized in LysoTracker-positive compartments (Fig 6B). To ensure that Ca²⁺ increase was exclusively from intracellular sources, all responses were measured in a “zero”-Ca²⁺ recording solution (Garrity *et al*, 2016), unless otherwise noted. TRPML1-GCaMP6m fluorescence responded preferentially and reliably to Ca²⁺ release from lysosomes induced by GPN (50 μM , Fig EV3A) or ML-SA1 (20 μM , Fig EV3B), but not to cytosolic Ca²⁺ increase triggered by an inhibitor of the sarco/endoplasmic reticulum Ca²⁺ ATPase (SERCA), thapsigargin (2 μM , Fig EV3C and D), which is consistent with previously reported results in COS-1 cells (Shen *et al*, 2012). Together, these results show that TRPML1-GCaMP6m readily and preferentially detects lysosomal Ca²⁺ release.

We next transfected TRPML1-GCaMP6m in HeLa cells with LAMTOR1 KD performed with transient CRISPR/Cas9 transfection (Fig EV3E and F). ML-SA1 elicited a significantly larger Ca²⁺ signal in cells with LAMTOR1 KD than in control cells (Fig 6C). Treatment with TAT-2031 (10 μM , 2 h), but not control TAT, significantly

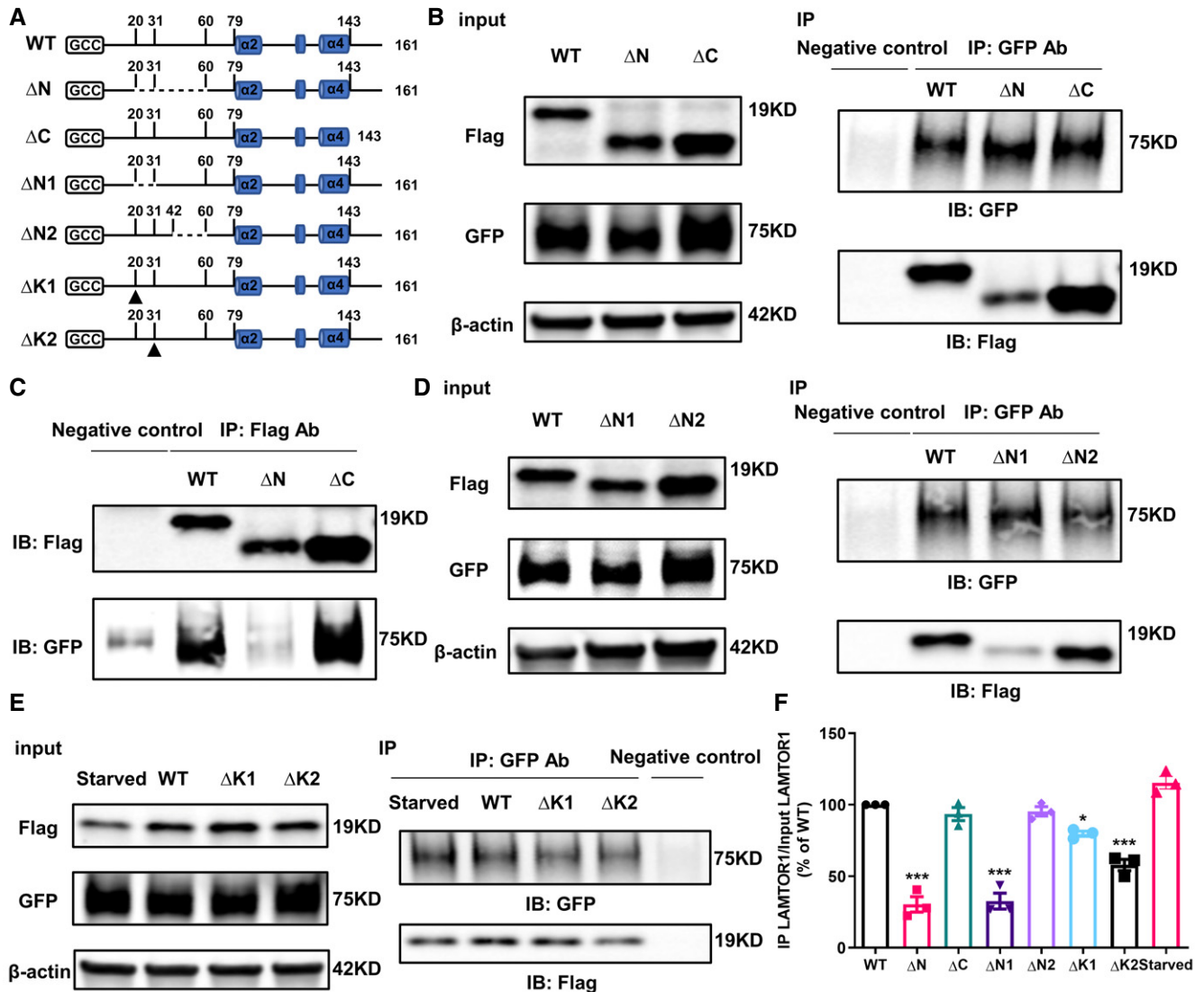


Figure 4. Characterization of the interaction between LAMTOR1 and TRPML1.

A Schematic structure of LAMTOR1 mutants. GCC are lipidation sites. Blue cans indicate α -helices. Dashed lines indicate the locations of amino acid deletions. Arrowheads indicate the locations of amino acid substitutions. WT, wild-type; Δ N, N-terminal deletion; Δ C, C-terminal deletion; Δ K1, K20R; Δ K2, K31R.

B-E Lysates from HeLa cells cotransfected with LAMTOR1-Flag or its mutants (Δ N and Δ C in B, Δ N1, and Δ N2 in D, Δ K1, and Δ K2 in E) and TRPML1-YFP were immunoprecipitated with anti-GFP or control IgG antibodies and probed with the indicated antibodies. Left, input proteins; right, immunoprecipitated (IP) proteins. Note one group (Starved) of HeLa cells transfected with LAMTOR1-Flag and TRPML1-YFP in (E) were incubated in medium without amino acids and serum for 2 h.

(C) Lysates from HeLa cells transfected as described in (B) were immunoprecipitated with anti-Flag or control IgG antibodies and probed with Flag and GFP antibodies. See Appendix Fig S4 for negative controls.

F Quantification of co-IP results. $N = 3$ independent experiments.

Data information: Data with error bars are represented as means \pm SEM. Statistical significance was assessed by one-way ANOVA with Dunnett's post-test (F). * $P < 0.05$, *** $P < 0.001$. See also Fig EV2 and Appendix Fig S4. Source data are available online for this figure.

increased TRPML1-mediated Ca^{2+} signals induced by ML-SA1 (Fig 6D and E). Likewise, deletion of LAMTOR1 N-terminal amino acids 20–31 also significantly increased ML-SA1-elicited Ca^{2+} signal in HeLa cells (Fig EV3G).

In cultured neurons, TRPML1-GCaMP6m was also mainly localized in LysoTracker-positive compartments (Fig 6F, Mander's coefficient, 0.76 ± 0.05 , $n = 7$). Pretreatment with GPN or with the

highly selective Ca^{2+} chelator, BAPTA-AM, abolished ML-SA1-elicited responses, confirming that TRPML1-GCaMP6m locally responds to lysosomal Ca^{2+} release in neurons (Fig 6G and H). ML-SA1-induced Ca^{2+} release was blocked by ML-SI1 (Fig 6G and H). As in HeLa cells, TRPML1-GCaMP6m did not significantly respond to cytosolic Ca^{2+} increase induced by either thapsigargin or ionomycin under low external Ca^{2+} , while it did respond to massive Ca^{2+} influx

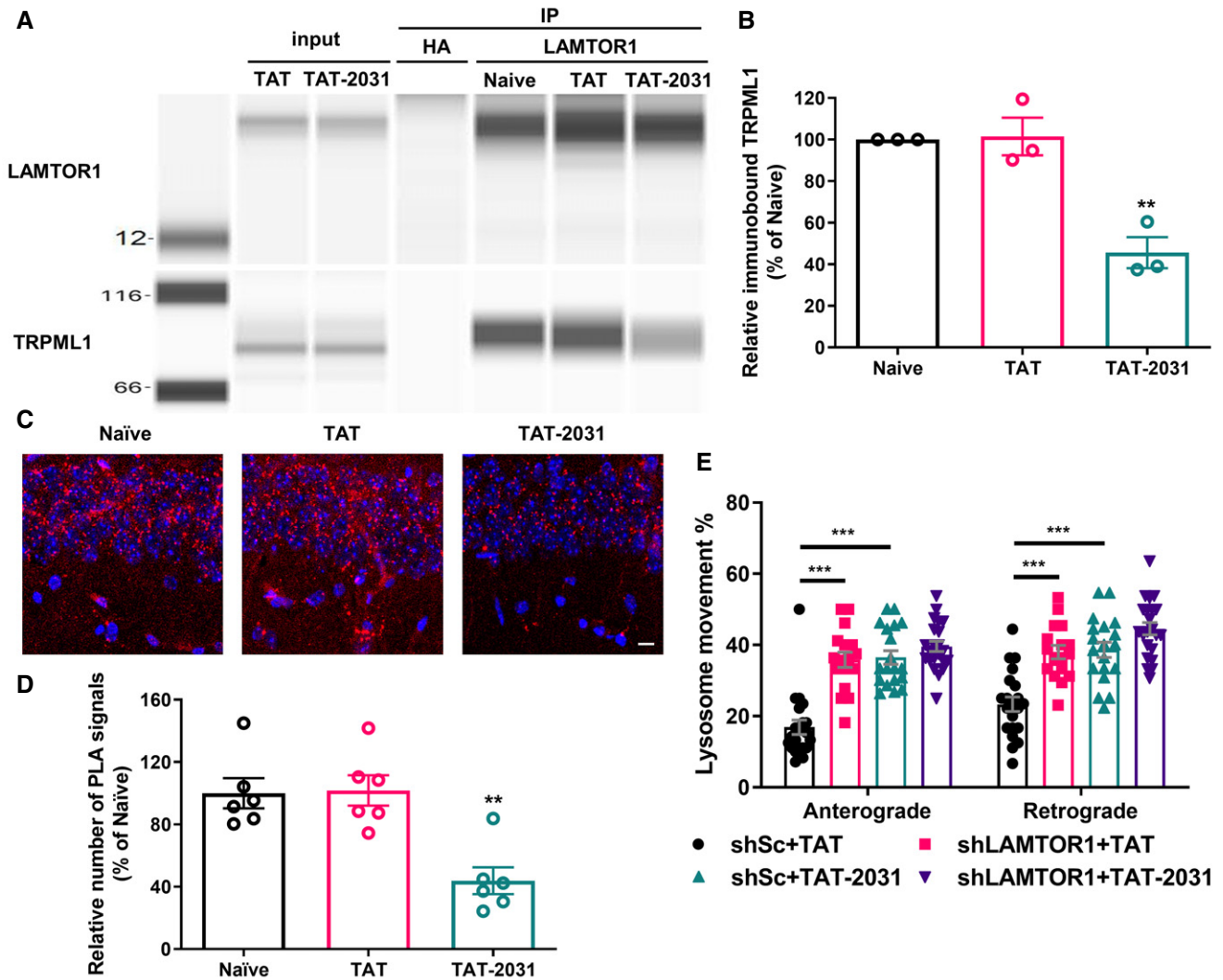


Figure 5. Effects of TAT-2031 on the interaction between LAMTOR1 and TRPML1 *in vivo* and lysosomal trafficking in dendrites of hippocampal neurons.

A Interactions between LAMTOR1 and TRPML1 in mouse hippocampus. Binding of LAMTOR1 to TRPML1 *in vivo* was disrupted by systemic administration of the TAT-2031 peptide. Wes protein analysis with anti-LAMTOR1 and -TRPML1 antibodies of immunoprecipitation performed with anti-LAMTOR1 antibodies or negative control anti-HA antibodies using whole hippocampal homogenates from naïve, TAT or TAT-2031-treated mice.

B Quantification of the relative abundance of TRPML1 pulled down by LAMTOR1 in naïve, TAT or TAT-2031-treated mice. *N* = 3 mice for each group.

C Representative images from proximity ligation assay (PLA) performed on brain slices from naïve, TAT or TAT-2031-treated mice. Evidence of proximity between LAMTOR1 and TRPML1 is indicated by the appearance of red puncta. Nuclei are counterstained with DAPI (blue). Scale bar, 10 μ m. See Appendix Fig S5E for negative controls.

D Quantification of the number of PLA signals in CA1 from naïve, TAT or TAT-2031-treated mice. *N* = 6 mice for each group.

E TAT-2031 treatment increased lysosomal mobility. Neurons were infected with shLAMTOR1 or shSc AAV; they were treated with TAT or TAT-2031 (10 μ M) and imaged with LysoTracker to visualize lysosomal trafficking in dendrites. *N* = 17–22 neurons from 3 independent experiments.

Data information: Data with error bars are represented as means \pm SEM. Statistical significance was assessed by one-way ANOVA with Dunnett's post-test (B, D), or two-way ANOVA with Tukey's post-test (E). ***P* < 0.01, ****P* < 0.001. See also Fig EV2 and Appendix Figs S3 and S5. Source data are available online for this figure.

induced by ionomycin under high external Ca^{2+} (Fig EV3H). In contrast, BioTracker 609 Red Ca^{2+} AM Dye detected cytosolic Ca^{2+} increase regardless of external Ca^{2+} concentration (Fig EV3H). These results indicate that TRPML1-GCaMP6m selectively responds to lysosomal Ca^{2+} release in neurons.

We next determined the effect of LAMTOR1 KD on TRPML1-mediated Ca^{2+} release in neurons using LAMTOR1 shRNA AAV

(mCherry reporter, Fig EV3I). LAMTOR1 KD significantly increased ML-SA1-elicited TRPML1-GCaMP6m Ca^{2+} signals. TAT-2031 treatment (10 μ M) also significantly increased Ca^{2+} signals as compared to control TAT treatment (Fig 5I). Of note, TAT-2031 treatment in LAMTOR1 KD neurons prolonged the Ca^{2+} signal wave (Fig EV3J), without further increasing its peak (Fig 6I and J). To further investigate LAMTOR1-mediated TRPML1 regulation in a more physiological

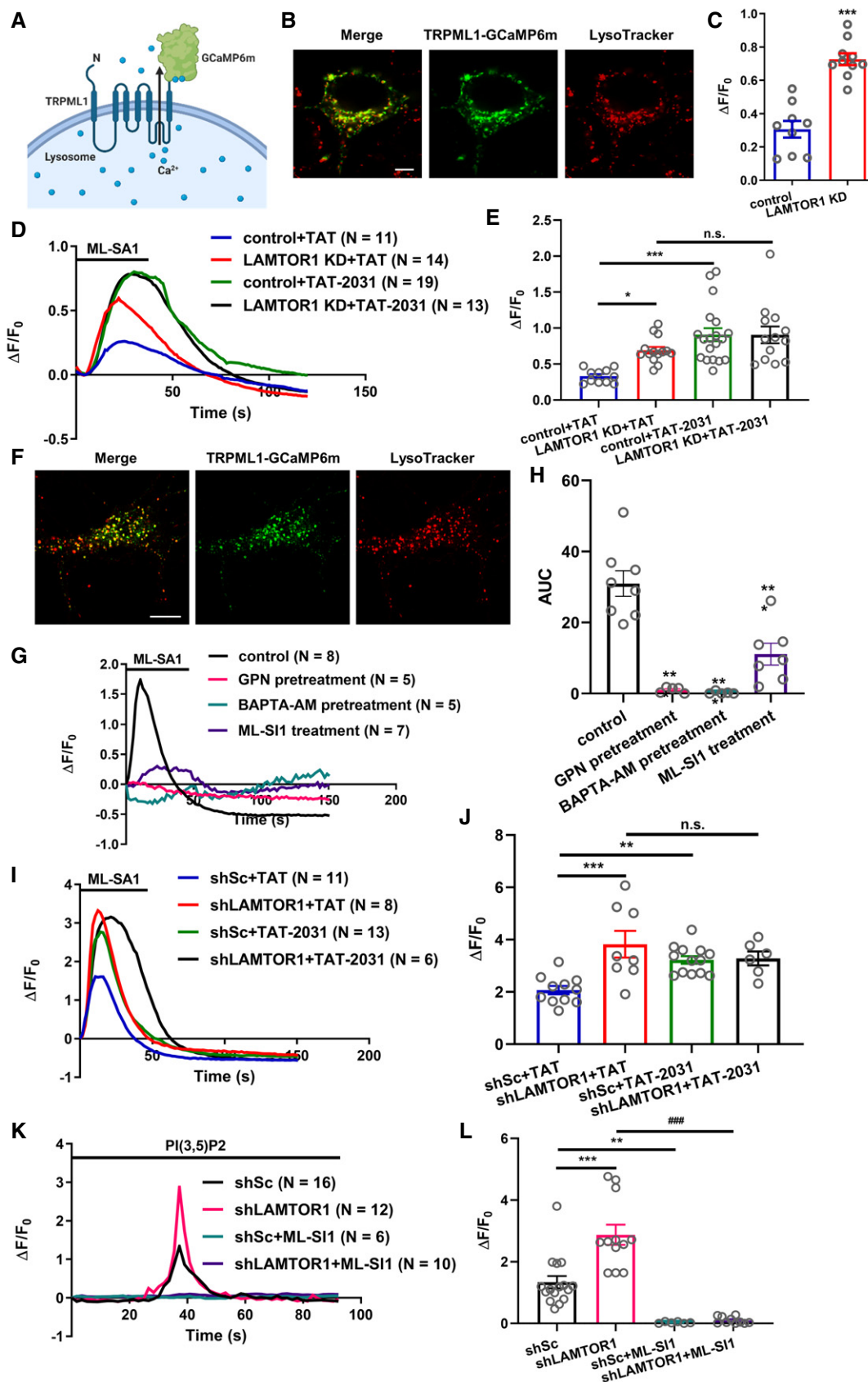


Figure 6.

Figure 6. Detection of TRPML1-mediated lysosomal Ca²⁺ release and its regulation by LAMTOR1.

- A Structure of the TRPML1-GCaMP6m-based Ca²⁺ sensor.
 B Colocalization of TRPML1-GCaMP6m (green) with LysoTracker (red) in HeLa cells. Scale bar, 5 μm.
 C ML-SA1 (20 μM)-induced peak GCaMP6m responses ($\Delta F/F_0$) were increased in CRISPR-Cas9-mediated LAMTOR1 KD cells. *N* = 9–10 cells from 4 independent experiments.
 D TAT-2031 treatment (10 μM) increased ML-SA1-induced TRPML1 Ca²⁺ release in both control and LAMTOR1 KD cells.
 E Quantification of peak responses as shown in (D). *N* = 11–19 cells from 5 independent experiments.
 F Colocalization of TRPML1-GCaMP6m (green) with LysoTracker (red) in hippocampal neurons. Scale bar, 10 μm.
 G Treatment with GPN (200 μM), BAPTA-AM (20 μM), or ML-SI1 (20 μM) blocked ML-SA1-induced TRPML1-GCaMP6m responses in neurons.
 H Quantification of responses in (G). *N* = 5–8 cells from 3 independent experiments.
 I Both LAMTOR1 KD and TAT-2031 treatment (10 μM) increased ML-SA1-induced TRPML1-GCaMP6m responses in neurons.
 J Quantification of peak responses as shown in I. *N* = 6–13 cells from 3 independent experiments.
 K LAMTOR1 KD increased PI(3,5)P2 (0.5 μM)-induced TRPML1-GCaMP6m responses and the blocking effect of ML-SI1 treatment (20 μM).
 L Quantification of peak TRPML1-GCaMP6m responses as shown in (K). *N* = 6–16 cells from 3 independent experiments.

Data information: Data with error bars are represented as means ± SEM. Statistical significance was assessed by Student's *t*-test (C), two-way ANOVA with Tukey's post-hoc analysis (E, J, L), and one-way ANOVA with Dunnett's post-test (H). **P* < 0.05, ***P* < 0.01, ****P* < 0.001, *****P* < 0.001, n.s., not significant. Note that the traces in D, G, I, and K represent the mean values of each group. See also Fig EV3.

Source data are available online for this figure.

context, we examined TRPML1 activity elicited by its endogenous activator, PI(3,5)P2 (0.5 μM). LAMTOR1 KD neurons exhibited significantly larger PI(3,5)P2-elicited TRPML1-GCaMP6m Ca²⁺ signals, as compared to control neurons, and ML-SI1 treatment (20 μM) completely abolished Ca²⁺ signals in both control and LAMTOR1 KD neurons (Fig 6K and L). Together, these results strengthen the notion that LAMTOR1 inhibits TRPML1 Ca²⁺ release, through direct interaction.

LAMTOR1 KD reduces LTP and enhances LTD in field CA1 of hippocampus by increasing TRPML1-induced calcineurin activation

Ca²⁺ plays critical roles in synaptic plasticity and learning and memory. More recently, it has been shown that lysosomes can traffic into dendritic spines in an activity-dependent manner (Goo *et al*, 2017) and that activity-dependent lysosomal exocytosis regulates structural plasticity of dendritic spines, an effect which requires lysosomal Ca²⁺ release (Padamsey *et al*, 2017). To investigate potential functions of LAMTOR1-mediated regulation of TRPML1 in synaptic plasticity, we determined the effects of the TRPML1 inhibitor ML-SI1 on long-term potentiation (LTP) and long-term depression (LTD) in acute hippocampal slices from control and LAMTOR1 shRNA-injected mice. AAV LAMTOR1 shRNA or scrambled shRNA were bilaterally injected into the dorsal hippocampal CA1 region of mice, and LTP/LTD was analyzed 4 weeks later. To evaluate

infection efficiency, GFP expression and LAMTOR1 levels were analyzed in hippocampal slices by immunohistochemistry (Fig EV4A). Levels of the lysosome-related proteins, LAMTOR1, LAMTOR2, TRPML1, LAMP2, cathepsin B, cathepsin D, and Rab7, were analyzed by Western blots (Fig EV4B and C). As previously reported (Sun *et al*, 2018), the amplitude of theta-burst stimulation (TBS)-induced LTP in field CA1 of hippocampal slices from LAMTOR1 shRNA-injected mice was significantly reduced, as compared to control shRNA-injected mice (Fig 7A and B). Pre-incubation of hippocampal slices from LAMTOR1 shRNA-injected mice with ML-SI1 (20 μM) eliminated the effects of LAMTOR1 KD on TBS-induced LTP (Fig 7A and B). ML-SI1 at this concentration did not affect TBS-induced LTP in slices from control shRNA-injected mice (Fig 7A and B), nor did it affect baseline synaptic responses (Fig EV5A–C) or paired-pulse facilitation (Fig EV5D) in slices from either control shRNA or LAMTOR1 shRNA-injected mice.

Low-frequency stimulation (LFS; 1 Hz, 15 min) of the Schaffer collaterals in hippocampal slices from 3-month-old control shRNA-injected mice only induced a transient synaptic depression (Fig 7C and D), which is consistent with the literature regarding the lack of stable LTD in adult mice (Dudek & Bear, 1993; Wagner & Alger, 1995; Guo *et al*, 2012; Sun *et al*, 2015; Pinar *et al*, 2017). However, the same protocol induced sustained LTD in slices from LAMTOR1 shRNA-injected mice (Fig 7C and D). ML-SI1 (20 μM) pre-treatment significantly reduced LTD in slices from LAMTOR1 shRNA-injected

Figure 7. LAMTOR1 KD reduces LTP and enhances LTD in field CA1 of hippocampus by increasing TRPML1-mediated Ca²⁺ release and calcineurin activation.

- A–D Effects of LAMTOR1 KD and ML-SI1 treatment on TBS-induced LTP (A) or LFS-induced LTD (C) in CA1. (B, D) Means ± SEM of fEPSPs measured 40 min after TBS (B, *n* = 4–5 slices from 4 to 5 mice) or LFS (D, *n* = 4–8 slices from 4 to 8 mice) in different groups.
 E Effects of ML-SI1 treatment on LFS-induced LTD in CA1 from 2- to 3-weeks-old mice.
 F Means ± SEM of fEPSPs measured 45 min after LFS in different groups. *N* = 6–8 slices from 6 to 8 mice.
 G–J Effects of TAT-2031 treatment on TBS-induced LTP (G) or LFS-induced LTD (I) in CA1. H, J Means ± SEM of fEPSPs measured 40 min after TBS (H, *n* = 6 slices from 6 mice) or LFS (J, *n* = 3–4 slices from 3 to 4 mice) in different groups.
 K Effects of LAMTOR1 KD and treatment with a calcineurin inhibitor, FK506, on LFS-induced LTD in CA1.
 L Means ± SEM of fEPSPs measured 45 min after LFS in different groups (*n* = 3–4 slices from 3 to 4 mice).

Data information: Slopes of fEPSPs were normalized to the average values recorded during the first 10-min baseline (A, C, E, G, I, K). Statistical significance was assessed by two-way ANOVA with Tukey's post-test (B, D, L) and Student's *t*-test (F, H, J). **P* < 0.05, ***P* < 0.01, ****P* < 0.001 compared with shSc, Vehicle, or TAT, #*P* < 0.05, ##*P* < 0.01, ###*P* < 0.001 compared with shLAMTOR1. Insets show representative traces of evoked fEPSPs before and 40 min after TBS/LFS. Scale bar 0.5 mV/10 ms. See also Figs EV4 and EV5.

Source data are available online for this figure.

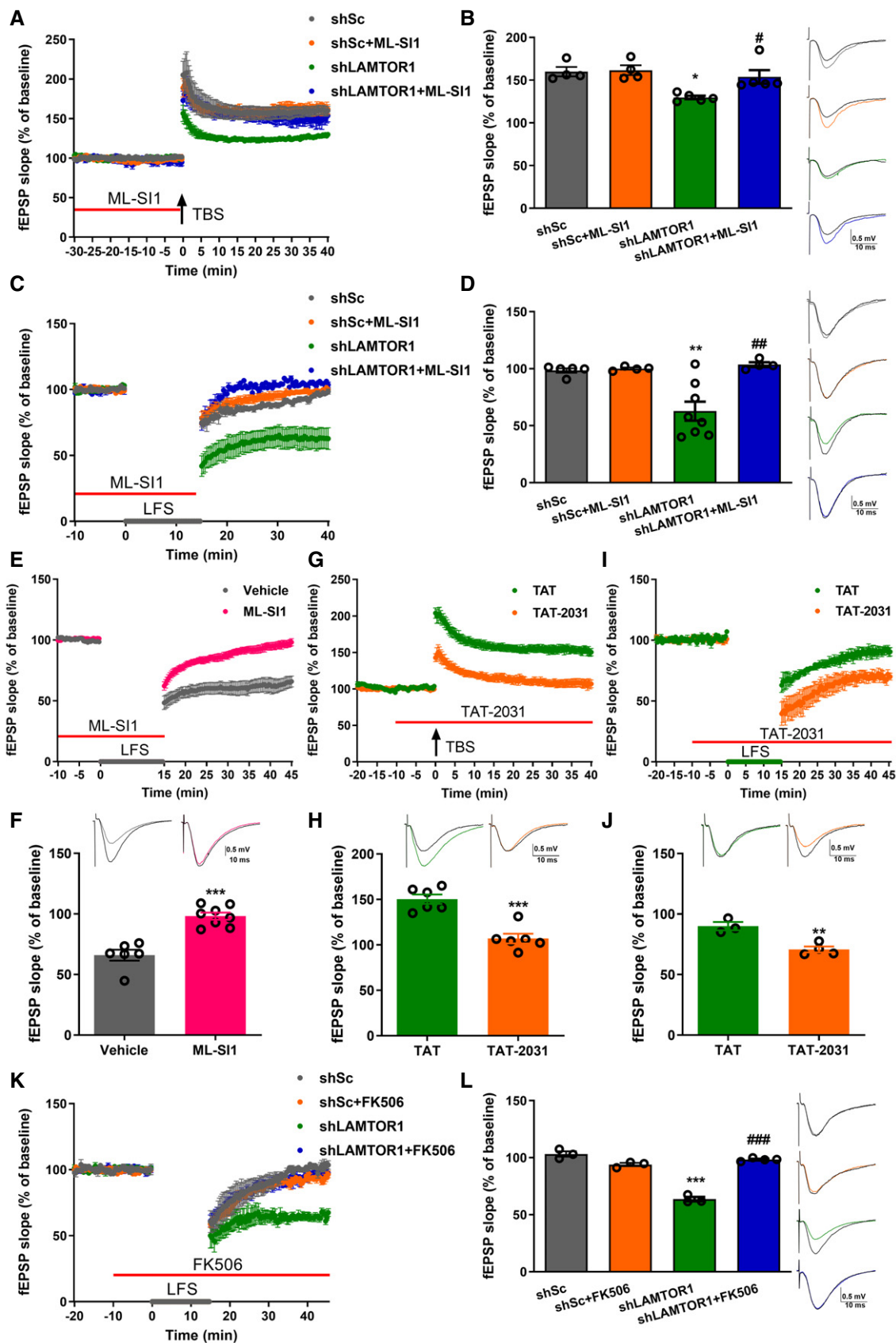


Figure 7.

mice and did not affect the transient depression in slices from control siRNA-injected mice (Fig 7C and D). Notably, ML-SI1 (20 μ M) pre-treatment significantly reduced LTD in hippocampal slices from 2- to 3-weeks-old mice (Fig 7E and F), suggesting that TRPML1-mediated Ca^{2+} release plays an important role in the formation of stable LTD in young animals. Pretreatment of hippocampal slices from adult mice with TAT-2031 (10 μ M) mimicked LAMTOR1 KD and significantly reduced TBS-induced LTP and enhanced LFS-induced LTD, while the control TAT peptide had no effect (Fig 7G–J).

Lysosomal Ca^{2+} release through TRPML1 can activate calcineurin (CaN) (Medina *et al*, 2015), which plays a critical role in LTD (Beattie *et al*, 2000; Baumgartel & Mansuy, 2012). Inhibition of CaN with FK506 (50 μ M) significantly reduced LTD in hippocampal slices from LAMTOR1 shRNA-injected adult mice (Fig 7K and L). Since CaN regulates synaptic plasticity by dephosphorylation of GluA1 at Ser845 (Beattie *et al*, 2000), and dephosphorylation of AMPA receptors results in their lysosomal degradation, which is also involved in LTD (Fernandez-Monreal *et al*, 2012), we analyzed phosphoSer845-GluA1 and total GluA1 in hippocampal CA1 stratum radiatum (SR) from control or LAMTOR1 shRNA-injected mice 30 min after LFS. Levels of phosphoSer845-GluA1 and total GluA1 were significantly lower in LAMTOR1 shRNA-injected mice, as compared with control shRNA-injected mice. Application of ML-SI1 10 min before LFS and maintained during LFS had no effect in slices from control shRNA-injected mice but significantly increased phosphoSer845-GluA1 and GluA1 levels in slices from LAMTOR1 shRNA-injected mice (Fig 8A–C and Appendix Fig S6A–D). Notably, the ratio of phosphoSer845-GluA1 to total GluA1 was also significantly lower in LAMTOR1 KD slices as compared with control slices, and this effect was reversed by ML-SI1 treatment (Fig 8D). LAMTOR1 KD also significantly reduced phosphoSer845-GluA1 levels in cultured hippocampal neurons, and this effect was reversed by ML-SI1 treatment (20 μ M, 2.5 h) (Appendix Fig S6E and F). These results indicate that LAMTOR1 KD-induced TRPML1 Ca^{2+} release and CaN activation contribute to GluA1 dephosphorylation and subsequent degradation.

To test whether increased lysosomal degradation was involved in the reduction of GluA1 levels in LAMTOR1 KD dendrites, we performed double immunolabeling with antibodies against GluA1 and LAMP2, a well-characterized lysosomal marker (Eskelinen, 2006) in cultured neurons. Our results showed that GluA1 was colocalized with LAMP2 in dendrites (Fig 8E), and that more

GluA1/LAMP2 double-stained puncta were detected in LAMTOR1 KD than in control neurons, and this effect was reversed by ML-SI1 treatment (Fig 8E and F). These results provide potential mechanism for the decrease in GluA1 level observed in hippocampal slices.

LAMTOR1 KD-induced learning and memory impairment in mice is ameliorated by TRPML1 inhibition

To determine whether LAMTOR1 KD could affect learning and memory and whether the effect was mediated by TRPML1, we administered ML-SI1 (10 mg/kg, i.p.) to control and LAMTOR1 shRNA-injected mice 1 h before the training session and tested the various groups of mice in long-term (24-h retention) object recognition memory. LAMTOR1 shRNA-injected mice exhibited a significant impairment in long-term object memory, as compared to control mice (Fig 9A). In contrast, ML-SI1-treated LAMTOR1 KD mice performed similarly to control mice (Fig 9A). We next tested the effects of ML-SI1 on fear-conditioning. Control shRNA and LAMTOR1 shRNA-injected mice were treated with ML-SI1 (10 mg/kg, i.p.) 1 h before the training session. LAMTOR1 KD mice exhibited deficits in context-dependent but not in tone-dependent fear conditioning (Fig 9B and Appendix Fig S6G). ML-SI1 treatment significantly enhanced learning performance in LAMTOR1 KD mice, while it did not affect learning in control mice (Fig 9B). Additionally, there was no difference in freezing time in the preconditioning period, before or during tone application in the testing period between all experimental groups (Fig 9B and Appendix Fig S6G). These results showed that LAMTOR1 KD in hippocampus resulted in learning and memory impairment in object recognition and contextual fear conditioning paradigms and that the impairment was reversed by TRPML1 inhibition.

Discussion

Our results provide strong evidence that LAMTOR1, in conjunction with other Ragulator members, is a negative regulator of the lysosomal Ca^{2+} channel, TRPML1. Under normal conditions, LAMTOR1 tonically inhibits TRPML1-mediated Ca^{2+} release; LAMTOR1 KD releases this inhibition resulting in increased lysosomal Ca^{2+} release, which stimulates dynein-dependent lysosome trafficking along bidirectionally oriented microtubules in dendrites (Fig 9C). Following LAMTOR1 KD, TRPML1-mediated Ca^{2+} release is also increased

Figure 8. Effects of LAMTOR1 KD and ML-SI1 treatment on GluA1 phosphorylation and levels in hippocampal neurons.

- A–D LAMTOR1 KD significantly reduced levels of GluA1 phosphorylation and total GluA1 as well as the ratio of p-GluA1 to GluA1 in hippocampal neurons, and this effect was reversed by ML-SI1 treatment. (A) Representative images of CA1 pyramidal neurons stained with anti-p-GluA1 S845 (magenta), anti-GluA1 (red), and anti-GFP (green) antibodies. Scale bar = 20 μ m. (B, C, D) Quantitative analysis of the mean fluorescence intensity (MFI) of p-GluA1 S845 (B), GluA1 (C)-immunoreactivity, and the ratio of p-GluA1 to GluA1 (D) in hippocampal CA1 stratum radiatum (SR) 30 min after LFS. $N = 4–6$ slices from 4 to 6 mice.
- E Representative images of proximal dendrites of hippocampal neurons stained with anti-GluA1 (green), anti-LAMP2 (red), and anti-GFP (gray) antibodies. Note that GluA1 labeled with Alexa Fluor 633 secondary antibodies was false-colored green and GFP false-colored gray to better show colocalization of GluA1 with LAMP2. Arrowheads indicate clearly colocalized puncta. Scale bar, 5 μ m.
- F Quantitative analysis of the ratio of the number of GluA1/LAMP2 colocalized puncta to that of total lysosomes in (F) ($n = 17–29$ neurons from 3 independent experiments).

Data information: Data with error bars are represented as means \pm SEM. * $P < 0.05$, ** $P < 0.01$ compared with shSc, # $P < 0.05$, ## $P < 0.01$ compared with shLAMTOR1; two-way ANOVA with Tukey's post-test (B, C, D, F). A.U., Arbitrary unit. See also Appendix Fig S6.

Source data are available online for this figure.

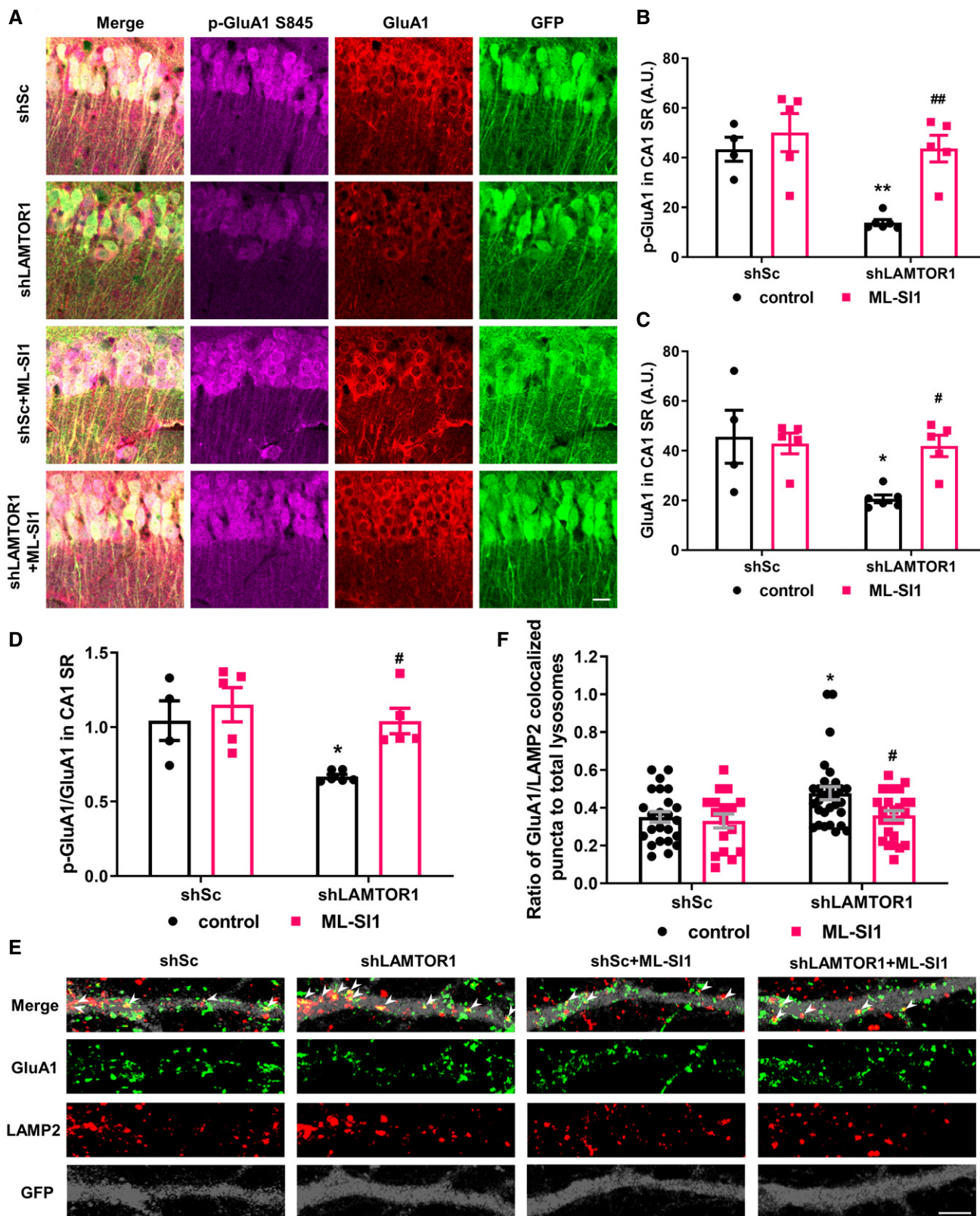


Figure 8.

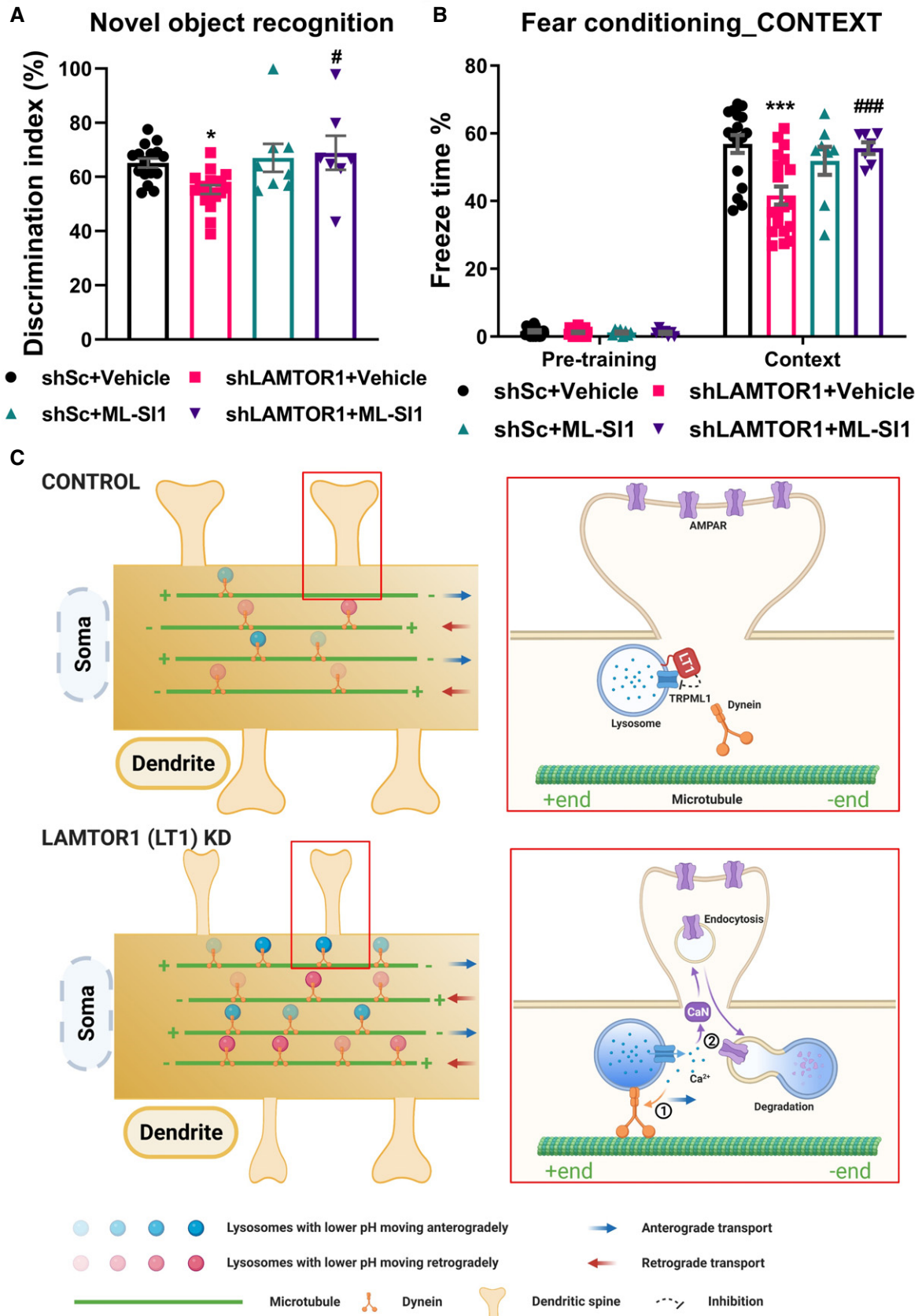


Figure 9.

Figure 9. LAMTOR1 KD-induced learning and memory impairment in mice is ameliorated by TRPML1 inhibition.

- A Mice received 10 min of training in an environment with two identical objects and received a retention test 24 h later in which one object was replaced with a novel one. LAMTOR1 shRNA-injected mice exhibited a significant deficit 24 h after training, which was reversed by ML-SI1 treatment ($N = 7-18$ mice).
- B % freezing for different experimental groups in context memory ($N = 7-19$ mice).
- C Model illustrating the proposed role of LAMTOR1-mediated inhibition of lysosomal Ca^{2+} release via TRPML1 in the regulation of lysosome motility in dendrites and synaptic plasticity. More lysosomes with lower pH move faster and longer distances in LAMTOR1 KD neurons, as compared to control neurons. LAMTOR1 interaction with TRPML1 inhibits its Ca^{2+} release and LAMTOR1 KD increased its Ca^{2+} release and dynein-dependent dendritic lysosome trafficking (①). LAMTOR1 KD-induced TRPML1 Ca^{2+} release also activates CaN, efficiently dephosphorylating GluA1 and targeting internalized AMPARs to lysosomes for degradation, thereby regulating synaptic plasticity (②). Figs 3B and 5A, and 8C were created with BioRender.com.

Data information: Data with error bars are represented as means \pm SEM. Statistical significance was assessed by two-way ANOVA with Tukey's post-test. * $P < 0.05$, *** $P < 0.001$, as compared to shSc; # $P < 0.05$, ### $P < 0.001$, as compared to shLAMTOR1. See also Appendix Fig S6G.

Source data are available online for this figure.

from lysosomes located in the vicinity of synapses, which results in CaN activation and GluA receptor dephosphorylation, endocytosis, and degradation, possibly through enhanced fusion of endosomes with acidic/degradative lysosomes made more available as a result of enhanced trafficking (Fig 9C). These processes reshape synaptic plasticity, that is, favoring LTD induction but impeding LTP consolidation as well as learning and memory.

We showed that enhanced TRPML1-mediated Ca^{2+} release, either by stimulation with the specific agonist, ML-SA1, or by disinhibition from LAMTOR1, facilitates both centripetal and centrifugal lysosomal trafficking in a dynein-dependent manner, which is consistent with the microtubule arrangement in dendrites of mature neurons with both outward and inward plus to minus end orientations (Baas *et al*, 1988; Kapitein *et al*, 2010; Tas *et al*, 2017). Thus, our results clearly showed that like in non-neuronal cells (Li *et al*, 2016), TRPML1 activation plays an important role in lysosomal trafficking in neuronal dendrites. The facilitated lysosomal trafficking was selectively blocked by the dynein inhibitor ciliobrevin D, which suggests that the same machinery described in non-neuronal cells, TRPML1-mediated Ca^{2+} release, ALG2 binding, and dynein-mediated trafficking, is operational in neuronal dendrites. Intriguingly, detailed quantification of mobile lysosomes revealed that LAMTOR1 KD-induced TRPML1 activation specifically increased the velocity and travel distance of the subpopulation of lysosomes with higher acidity (Fig 1D and E). Similarly, LAMTOR1 KD increased the mobile fraction of the degradative lysosomes with active cathepsin B (Fig 1H). Degradative lysosomes have been elegantly shown to be delivered to distal axons to maintain local degradation capacity (Farfel-Becker *et al*, 2019). It is thus tempting to speculate that these lysosomes would reach both the soma and synapses faster, which could facilitate local exchange of cargo contents, such as AMPARs, and their degradation. Along this line, Rab7 has been shown to play critical roles in the transport of dendritic cargos to proteolytically active lysosomes in the soma and proximal dendrites for degradation (Yap *et al*, 2018). Whether TRPML1-mediated lysosomal trafficking interacts with Rab7-mediated transport remains an interesting question. Interestingly, a recent paper showed that the actin network and myosin also regulate dendritic lysosomal trafficking by stalling lysosomes in the vicinity of synapses (van Bommel *et al*, 2019). Whether this mechanism cross talks with LAMTOR-TRPML1-mediated regulation is another interesting question.

We provided several lines of evidence indicating that LAMTOR1 negatively regulates TRPML1-mediated lysosomal Ca^{2+}

release by direct protein-protein interactions. LAMTOR1 binds to TRPML1 both in Hela cells and in hippocampal neurons through a sequence from K20 to K31 in the N-terminal domain of LAMTOR1. Genetic deletion or pharmacological inhibition of TRPML1 fully restored normal dendritic lysosomal trafficking in LAMTOR1 KD neurons, while TRPML1 activation by ML-SA1 mimicked the effects of LAMTOR1 KD. Finally, disruption of the interaction between LAMTOR1 and TRPML1 by a peptide specifically targeting the TRPML1 binding domain of LAMTOR1 mimicked the effects of LAMTOR1 KD. Of note, this peptide did not affect the association of LAMTOR1 with other members of the Ragulator or the activity of mTORC1. Together with the finding that LAMTOR2 KD mimicked the effects of LAMTOR1 KD on lysosomal trafficking, these results indicate that LAMTOR1, while associated with other Ragulator members, directly inhibits TRPML1 independently of mTOR. This conclusion is also supported by the finding that inhibition of mTORC1 by Raptor KD had no effect on lysosome motility. Along this line, it has been shown that the Ragulator inhibits BORC-mediated centrifugal lysosomal trafficking, independently of mTOR, by directly interacting with BORC (Filipek *et al*, 2017; Pu *et al*, 2017), while it facilitates endosome-to-Golgi trafficking, possibly by acting as a guanine nucleotide exchange factor (Shi *et al*, 2018). We showed that although the BORC complex is indispensable for the regulation of lysosomal trafficking in non-neuronal cells and in neuronal axons, it is unlikely to play a major role in LAMTOR1-mediated regulation of lysosomal trafficking in neuronal dendrites (Fig 3A). How the Ragulator interacts with different proteins in trafficking of different cargos remains to be addressed.

Functionally, our results showed that LAMTOR1 KD impaired LTP but enabled LTD induction in the CA1 region of adult hippocampus; both effects were blocked by TRPML1 inhibition, suggesting that activation of TRPML1 channels was responsible for these effects. Lysosomal Ca^{2+} efflux through TRPML1 has been shown to locally activate CaN in non-neuronal cells (Medina *et al*, 2015). The same downstream mechanism that has been previously shown to be involved in LTD induction and LTP inhibition, namely, CaN-mediated dephosphorylation of GluA1 (Beattie *et al*, 2000; Baumgartel & Mansuy, 2012) is also responsible for LAMTOR1 KD-induced changes in synaptic plasticity. GluA1 phosphorylation at Ser845 increases AMPAR insertion into synaptic membranes, thereby strengthening synaptic transmission, while Ser845 dephosphorylation triggers AMPAR internalization and decreases synaptic transmission (Mulkey *et al*, 1994; Man *et al*, 2007).

Dephosphorylation of GluA1 at Ser845 and increased colocalization of GluA1 with lysosomal markers also occurred in hippocampal neurons following LAMTOR1 KD. Since lysosomes with lower pH move faster and for longer distances in such neurons, our results support a model in which LAMTOR1 KD not only enhances TRPML1-mediated Ca^{2+} release, which facilitates CaN activation and GluA endocytosis, but also increases the fusion of GluA-containing endosomes with degradative lysosomes (Fernandez-Monreal *et al*, 2012). The same mechanism is also likely responsible for LAMTOR1 KD-induced impairment in long-term object recognition memory and context memory in the fear-conditioning paradigm since both forms of learning were restored by the administration of the TRPML1 inhibitor ML-SI1. Of note, our results indicate that this process is set in motion by either LFS, TBS, or learning activity; whether this process could affect basal synaptic transmission and AMPAR activity, if activated long enough, remains to be determined.

It has been consistently reported that LFS-induced LTD is readily recorded at the Schaffer collateral synapses in hippocampus of young (< 2–3 weeks old) rodents and becomes less robust and more difficult to induce thereafter (Dudek & Bear, 1993; Wagner & Alger, 1995; Pinar *et al*, 2017). We confirmed these findings and showed that LTD in juvenile hippocampus was blocked by the TRPML1 inhibitor, ML-SI1. Several hypotheses have been provided as the underlying mechanism for the developmental changes in LTD induction and expression (see Pinar *et al* (2017) for a recent review). Our results suggest changes in the regulation of TRPML1 activity as an additional potential mechanism.

We previously reported that LAMTOR1 KD reduced mTORC1 activity, reduced the number of mature spines, and resulted in LTP impairment (Sun *et al*, 2018). We also showed that pretreatment with an mTOR activator ameliorated LAMTOR1 KD-induced LTP impairment in hippocampal slices (Sun *et al*, 2018). These findings do not contradict the current results, since multiple signaling pathways, including mTORC1 as well as CaN, are involved in LTP and LTD (Malenka & Bear, 2004; Minichiello, 2009; Patterson & Yasuda, 2011; Baudry & Bi, 2016; Nicoll, 2017; Nakahata & Yasuda, 2018). It should also be noted that mTORC1 inhibits TRPML1 activity (Onyenwoke *et al*, 2015), which could be a potential mechanism for enhanced TRPML1 activation following LAMTOR1 KD. However, as discussed earlier, our results showed that TAT-2031 disrupted LAMTOR1-TRPML1 interactions and increased TRPML1 Ca^{2+} release without affecting mTORC1 activity. Thus, LAMTOR1 regulates synaptic plasticity through both mTORC1- and TRPML1-mediated signaling pathways.

In summary, our results indicate that LAMTOR1 is an endogenous negative regulator of the TRPML1 channels and that LAMTOR1-mediated tonic inhibition of TRPML1-mediated Ca^{2+} release is critical for maintaining normal dendritic lysosomal trafficking, synaptic plasticity, and learning and memory, as disruption of this inhibition leads to enhanced lysosomal mobility and abnormal plasticity and impaired learning and memory. Since lysosomal dysfunctions, including those induced by alterations in TRPML1 activity, have been implicated in various diseases (see Santoni *et al* (2020) for a recent review), these findings suggest that dysfunction of LAMTOR1-mediated TRPML1 regulation might be involved in various neurological and neuropsychiatric diseases.

Materials and Methods

Animals

Animal experiments were conducted in accordance with the principles and procedures of the National Institutes of Health Guide for the Care and Use of Laboratory Animals. All protocols were approved by the Institutional Animal Care and Use Committee of Western University of Health Sciences. Original mice were obtained from The Jackson Laboratory, strain B6129SF2/J (Stock No:101045), and a breeding colony was established. Both male and female mice aged between 2 and 4 months were used in all experiments except for one group in which 2–3-weeks-old mice were used for LTD experiment. Mice were housed in groups of two to three per cage and maintained on a 12-h light/dark cycle with food and water ad libitum.

Hippocampal neuronal cultures

Hippocampal neurons were prepared from E18 mouse embryos as described (Sun *et al*, 2015). Briefly, hippocampi were dissected and digested with papain (2 mg/ml, Sigma) for 30 min at 37°C. Dissociated cells were plated onto poly-L-lysine-coated 6-well plates at a density of $6\text{--}10 \times 10^4$ cells/cm² or confocal dishes/coverslips in 24-well plates at a density of $6\text{--}10 \times 10^3$ cells/cm² in Neurobasal medium (Gibco) supplemented with 2% SM1 (STEMCELL) and 2 mM glutamine and kept at 37°C under 5% CO₂. Half of the culture medium was replaced with BrainPhys medium (STEMCELL) supplemented with SM1 at DIV5 and then every 7 days.

Cell lines

Hela cells (ATCC) were grown in EMEM (ATCC) supplemented with 10% (vol/vol) fetal bovine serum (FBS) (Invitrogen) and kept at 37°C under 5% CO₂. Mouse embryonic fibroblasts (MEFs, gift from Dr. Jijun Hao, WesternU) were grown in DMEM (Gibco) supplemented with 10% (vol/vol) FBS and 0.1 mM β -mercaptoethanol (Sigma) and kept at 37°C under 5% CO₂.

Transfection and AAV infection

For transient expression of constructs, Hela cells and MEFs were transfected with the respective constructs by lipofection (Lipofectamine 2000; Invitrogen) according to the manufacturer's instructions.

Cultured hippocampal neurons were transfected with Accell LAMTOR1 siRNA or Accell Non-targeting siRNA (GE Dharmacon) at DIV4 and neurons were co-transfected with LAMP1-YFP 72 h after infection. Cultured neurons were used 24 h after the second transfection.

Cultured hippocampal neurons were infected with LAMTOR1 shRNA AAV, LAMTOR2 shRNA AAV, Raptor shRNA AAV, or scrambled shRNA AAV (Vector Biolabs) at DIV7, and 2/3 of the medium was replaced with fresh medium 24 h after infection. For the rescue experiment, LAMTOR1 shRNA AAV-infected neurons were infected with RNAi-resistant LAMTOR1 AAV (VectorBuilder) at DIV14. For TRPML1 or lyspersin KD experiment, neurons were co-transfected with Accell TRPML1 siRNA or lyspersin siRNA or control siRNA (GE Dharmacon) at DIV17. Neurons were analyzed at DIV21.

Antibodies, chemicals, and DNA constructs

Antibodies, chemicals, and plasmids used in this study are listed in Table 1. The following peptides were synthesized by ABI Scientific: TAT (YGRKKRRQRRR), and TAT-2031-h (human, YGRKKRRQRRRKLDPSSPPTK), and TAT-2031-m (mouse, YGRKKRRQRRRKLDPSSPPTK).

Expression constructs encoding LAMTOR1-Flag, pU6-(BbsI)_{CBh}-Cas9-T2A-mCherry, TRPML1-YFP, and LAMP1-YFP were

obtained from Addgene. LAMTOR1 fragments with N- or C-terminal deletions were synthesized by Integrated DNA Technologies. The LAMTOR1-Flag-ΔN, ΔC, ΔN1, and ΔN2 constructs were made by replacing LAMTOR1 full-length complementary DNA between the EcoRI and NotI sites of the LAMTOR1-Flag plasmid with the synthesized sequences. Constructs with K-R mutations (LAMTOR1-Flag-ΔK1/2) were generated from LAMTOR1-Flag by site-directed mutagenesis (Agilent). The TRPML1-GCaMP6m construct was made by NEBuilder HiFi DNA Assembly (New England Biolabs). The

Table 1. Antibodies, chemicals, and plasmids used in this study.

Reagent or Resource	Source	Identifier
Antibodies		
Rabbit monoclonal anti-LAMTOR1	Cell Signaling Technology	Cat#8975; RRID:AB_10860252
Rabbit polyclonal anti-LAMTOR1	Sigma-Aldrich	Cat#HPA002997; RRID:AB_1845531
Rabbit monoclonal anti-LAMTOR2	Cell Signaling Technology	Cat#8145; RRID:AB_10971636
Rabbit monoclonal anti-LAMTOR3	Cell Signaling Technology	Cat#8168; RRID:AB_10949501
Rabbit monoclonal anti-LAMTOR4	Cell Signaling Technology	Cat#12284; RRID:AB_2797870
Rabbit monoclonal anti-LAMTOR5	Cell Signaling Technology	Cat#14633; RRID:AB_2798547
Mouse monoclonal anti-Flag	Sigma-Aldrich	Cat# F1804; RRID:AB_262044
Rabbit monoclonal anti-Flag	Abcam	Cat# ab205606
Rat monoclonal anti-LAMP2	Abcam	Cat#ab13524; RRID:AB_2134736
Mouse monoclonal anti-LAMP2	Santa Cruz Biotechnology	Cat#sc-18822; RRID:AB_626858
Rabbit polyclonal anti-TRPML1	Alomone	Cat#ACC-081; RRID:AB_10915894
Mouse monoclonal anti-TRPML1	Santa Cruz Biotechnology	Cat#sc-398868
Rabbit monoclonal anti-mTOR	Cell Signaling Technology	Cat#2983; RRID:AB_2105622
Rabbit polyclonal anti-p-mTOR	Cell Signaling Technology	Cat#2971; RRID:AB_330970
Rabbit polyclonal anti-mTOR	Cell Signaling Technology	Cat#2972; RRID:AB_330978
Rabbit polyclonal anti-p-S6K1	Cell Signaling Technology	Cat#9205; RRID:AB_330944
Rabbit polyclonal anti-S6K1	Cell Signaling Technology	Cat#9202; RRID:AB_331676
Rabbit polyclonal anti-p-S6	Cell Signaling Technology	Cat#2215; RRID:AB_331682
Rabbit monoclonal anti-S6	Cell Signaling Technology	Cat#2217; RRID:AB_331355
Rabbit monoclonal anti-Raptor	Cell Signaling Technology	Cat#2280; RRID:AB_561245
Rabbit polyclonal anti-GluA1	EMD Millipore	Cat#AB1504; RRID:AB_2113602
Mouse monoclonal anti-GluA1	Thermo Fisher Scientific	Cat#MAS-27694; RRID:AB_2735203
Rabbit polyclonal anti-Phospho-Ser ⁸⁴⁵ GluA1	PhosphoSolutions	Cat#p1160-845; RRID:AB_2492128
Rabbit monoclonal anti-Rab7	Cell Signaling Technology	Cat#9367; RRID:AB_1904103
Goat polyclonal anti-Cathepsin B	R&D Systems	Cat#AF965; RRID:AB_2086949
Goat polyclonal anti-Cathepsin D	R&D Systems	Cat#AF1029; RRID:AB_2087094
Rabbit polyclonal anti-GFP	Abcam	Cat#ab290; RRID:AB_303395
Mouse monoclonal anti-GFP	Thermo Fisher Scientific	Cat#33-2600; RRID:AB_2533111
Chicken polyclonal anti-GFP	Thermo Fisher Scientific	Cat#A10262; RRID:AB_2534023
Mouse monoclonal anti-GAPDH (clone 6C5)	EMD Millipore	Cat#MAB374; RRID:AB_2107445
Mouse monoclonal anti-β-actin (clone AC-15)	Sigma-Aldrich	Cat#A5441; RRID:AB_476744
Goat anti-rabbit IgG IRDye [®] 680RD	LI-COR Biosciences	Cat#926-68071; RRID:AB_10956166
Goat anti-mouse IgG IRDye [®] 800CW	LI-COR Biosciences	Cat#926-32210; RRID:AB_621842
Goat anti-rat IgG IRDye [®] 680RD	LI-COR Biosciences	Cat#926-68076; RRID:AB_10956590
Donkey anti-mouse IgG AlexaFluor 594	Invitrogen	Cat#A-21203; RRID:AB_2535789

Table 1 (continued)

Reagent or Resource	Source	Identifier
Goat anti-rabbit IgG AlexaFluor 488	Invitrogen	Cat#A-11008; RRID:AB_143165
Goat anti-rabbit IgG AlexaFluor 594	Invitrogen	Cat#A-11037; RRID:AB_2534095
Donkey anti-rat IgG AlexaFluor 594	Invitrogen	Cat#A-21209; RRID:AB_2535795
Goat anti-chicken IgY AlexaFluor 488	Invitrogen	Cat#A-11039; RRID:AB_2534096
Goat anti-rabbit IgG AlexaFluor 633	Invitrogen	Cat#A-21070; RRID:AB_2535731
Donkey anti-goat IgG AlexaFluor Plus 594	Invitrogen	Cat#A-32758; RRID:AB_2762828
Chemicals, peptides, and recombinant proteins		
ML-SA1	Tocris	Cat#4746
ML-SI1	Alfa Aesar	Cat#J67425
ML-SI1	Sigma	Cat#G1421
Cilobrevin D	EMD Millipore	Cat#250401
GPN	Cayman Chemical	Cat#14634
Thapsigargin	Tocris	Cat#1138
Torin 1	Tocris	Cat#4247
FK506	Tocris	Cat#3631
TAT	ABI Scientific	Custom
TAT-2031-human	ABI Scientific	Custom
TAT-2031-mouse	ABI Scientific	Custom
Lipofectamine 2000	Invitrogen	Cat#11668019
LysoTracker Red DND-99	Invitrogen	Cat#L7528
Transferrin, Alexa Fluor 594 Conjugate	Invitrogen	Cat#T13343
BioTracker 609 Red Ca ²⁺ AM Dye	Sigma	Cat#SCT021
Shuttle PIP Kit, PI(3,5)P2	Echelon Biosciences	Cat#P-9035
Duolink® <i>In Situ</i> Red Starter Kit Mouse/Rabbit	Sigma	Cat#DUO92101
Recombinant DNA		
LAMTOR1-Flag	Bar-Peled <i>et al</i> (2012)	RRID:Addgene_42331
LAMTOR1-Flag ΔN	This paper	N/A
LAMTOR1-Flag ΔC	This paper	N/A
LAMTOR1-Flag ΔN1	This paper	N/A
LAMTOR1-Flag ΔN2	This paper	N/A
LAMTOR1-Flag ΔK1	This paper	N/A
LAMTOR1-Flag ΔK2	This paper	N/A
pU6-(BbsI)_CBh-Cas9-T2A-mCherry (CRISPR-Cas9 control plasmid)	Chu <i>et al</i> (2015)	RRID:Addgene_64324
CRISPR-Cas9 plasmid with sgRNA targeting <i>LAMTOR1</i>	This paper	N/A
TRPML1-YFP	Venkatachalam <i>et al</i> (2006)	RRID:Addgene_18826
TRPML1-GCaMP6m	This paper	N/A
LAMP1-YFP	Sherer <i>et al</i> (2003)	RRID:Addgene_1816
pGCaMP6m-N3-TPC2	Ambrosio <i>et al</i> (2015)	RRID:Addgene_80147

Further information and requests for resources and reagents should be directed to and will be fulfilled by Corresponding author.

GCaMP6m sequence cloned from TPC2-GCaMP6m was fused to the C-terminus of the TRPML1 sequence cloned from TRPML1-YFP. For transient co-expression of CRISPR/Cas9 components, LAMTOR1-sgRNA nucleotides were synthesized and cloned into pU6-(BbsI)_CBh-Cas9-T2A-mCherry vector at BbsI site (Ran *et al*, 2013). The 20-bp targeting sequence is 5'-TCCGCTCGCACTGATGAGCA-3'. All constructs were confirmed by sequencing.

Live cell imaging

LysoTracker Red DND-99 (100 nM) was dissolved in culture medium and loaded into cells for 1 h before imaging. Alexa Fluor 594-conjugated Transferrin was dissolved in LCIS containing 20 mM of glucose and 1% BSA and loaded into cells for 20 min before imaging (25 μg/ml). For labeling degradative lysosomes,

Magic Red Cathepsin B fluorogenic substrates (1:500) were applied to cells for 15 min at 37°C before imaging. Live-cell imaging was performed in complete medium (for LysoTracker, Magic Red, and LAMP1-YFP) or Live Cell Imaging Solution (LCIS, Invitrogen, for Transferrin) using a Zeiss LSM880 AiryScan confocal microscope equipped with a Plan-Apochromat 63×/1.4 oil immersion objective, and an environmental chamber set at 37°C and 5% CO₂. Images were acquired over a period of 4 min (LysoTracker and Magic Red) or 1 min (LAMP1-YFP and Transferrin) at 1-s intervals and processed by using software ZEN (Zeiss) including brightness adjustment, conversion of images to movies, and kymograph generation.

Kymograph analysis and track quantification in Imaris

Kymographs were generated using Zen or the KymographClear plugin for ImageJ (NIH) (Mangeol *et al*, 2016). Nonoverlapping proximal dendritic stretches of 40 μm length with comparable thickness across different experimental groups were traced, using the segmented line tool. Line thickness was chosen to cover the dendritic shaft, but to omit spines. From the generated kymographs, we manually counted the identifiable traces; whenever there was ambiguity in the individual traces, we went back to the movie to confirm the results. A track was categorized as “stationary” if its displacement was less than 2 μm. Mobile tracks were sorted into anterograde or retrograde categories depending on the net direction of the tracks. To further confirm these results, we used the KymographClear program to generate kymographs, which provides automatic color coding of the different directions of movement (Appendix Fig S1A). These two quantification methods generated comparable results (Appendix Fig S1B). In general, all identifiable lysosomes were analyzed and the total number of lysosomes within the dendritic shaft was estimated by summing the numbers of stationary, anterograde, and retrograde lysosomes. The percentages of different categories were presented. We also manually counted all visible lysosomes in the first frame of the time-lapse movie and ROI selected for kymograph analysis to confirm the results (Appendix Fig S1C).

The software Imaris (Bitplane) was used to create lysosomal moving tracks in dendrites and quantify track speed, track displacement length, and mean fluorescent intensity of mobile lysosomes in dendrites. Lysosomes within the dendritic segment were selected using spot function, and tracks were automatically created using the Brownian motion algorithm. Generated tracks were further validated by examiners blind to the experiment groups and adjusted to best fit the live images sequences. Only vesicles with track displacement length more than 2 μm were used for analysis. Nonmoving lysosomes, potentially interfering tracking, were excluded.

FRAP and quantification of lysosome movement

For FRAP experiments, neurons were incubated with LysoTracker as described above. After cells were imaged for 20 s at 1-s intervals, a region (5 μm × 15–20 μm) was selected for photobleaching, which was performed at 100% laser power (561 nm excitation) and 500 iterations using the Zen software bleaching mode. Images were acquired over a period of 4 min at 1-s intervals. Two lines were drawn at the two edges of each bleached area, and the number of

lysosomes crossing the line (proximal to soma) away from the soma (anterograde) and crossing the line (distal to soma) toward the soma (retrograde) during the 4-min imaging time was counted.

TRPML1-GCaMP6m Ca²⁺ imaging

HeLa cells were transfected with CRISPR-Cas9 plasmids (with mCherry reporter) with or without sgRNA targeting *LAMTOR1*, and 48 h later, cells were co-transfected with TRPML1-GCaMP6m. Cultured hippocampal neurons were infected with scrambled shRNA or *LAMTOR1* shRNA AAV with mCherry co-expression (UCI Center for Neural Circuit Mapping) at DIV1 for 7 days; they were then transfected with TRPML1-GCaMP6m at DIV7. Experiments were carried out within 18–24 h after transfection with TRPML1-GCaMP6m as previously described with modifications (Shen *et al*, 2012; Garrity *et al*, 2016). TRPML1-GCaMP6m fluorescence was monitored at an excitation wavelength of 488 nm using a Zeiss LSM880 AiryScan confocal microscope equipped with a 20× objective. Images were acquired over a period of 150 s at 1-s intervals and analyzed by using software ZEN (Zeiss). Cells were bathed in Tyrode's solution containing 145 mM of NaCl, 5 mM of KCl, 2 mM of CaCl₂, 1 mM of MgCl₂, 10 mM of Glucose, and 20 mM of Hepes (pH 7.4). Lysosomal Ca²⁺ release was measured in a zero Ca²⁺ solution containing 145 mM of NaCl, 5 mM of KCl, 3 mM of MgCl₂, 10 mM of glucose, 1 mM of EGTA, and 20 mM of HEPES (pH 7.4) (Garrity *et al*, 2016). Because baseline may drift after media changed from Tyrode's solution to zero Ca²⁺ solution, we typically set F₀ based on the value that is closest to the baseline. ML-SA1, GPN, and thapsigargin were applied to cells for indicated times (black lines in figures) and then washed out by applying a zero Ca²⁺ solution. When ML-S11 applied, it was present over the complete imaging period. PI(3,5)P₂ was delivered into cultured neurons at a concentration of 0.5 μM using Shuttle PIP kits following the manufacturer's protocol (Echelon Biosciences). Only mCherry-expressing cells were quantified.

Western blot analysis

For whole homogenates, tissue was homogenized in RIPA buffer (10 mM of Tris, pH 8, 140 mM of NaCl, 1 mM of EDTA, 0.5 mM of EGTA, 1% NP-40, 0.5% sodium deoxycholate, and 0.1% SDS). Cells were lysed with CHAPS lysis buffer (25 mM of Tris-HCl, pH 7.4, 150 mM of NaCl, 1 mM of EDTA, 0.5% CHAPS, 5% glycerol, and a protease inhibitor cocktail). Protein concentrations were determined with a BCA protein assay kit (Pierce). Western blots were performed according to published protocols (Sun *et al*, 2015). Briefly, samples were separated by SDS-PAGE and transferred onto a PVDF membrane (Millipore). After blocking with 3% BSA for 1 h, membranes were incubated with specific antibodies overnight at 4°C followed by incubation with IRDye secondary antibodies for 2 h at room temperature. Antibody binding was detected with the Odyssey[®] family of imaging systems (LI-COR Biosciences), and Western blots were analyzed with the Image Studio Software.

Immunoprecipitation

For immunoprecipitation, all procedures were carried out at 4°C. HeLa cells transfected with the indicated cDNAs were lysed with

CHAPS lysis buffer. The starvation protocol involved incubating the cells for 2 h with Earle's balanced salt solution (EBSS) before harvest. After a brief centrifugation to remove insoluble material, the supernatant was precleared with an aliquot of Dynabeads (Invitrogen). For immunoprecipitation of TRPML1-YFP in HeLa cells, extracts were incubated with anti-GFP Dynabeads, washed with washing buffer, followed by elution of bound proteins by incubating at 37°C for 30 min in SDS-PAGE sample buffer. For immunoprecipitation of LAMTOR1-Flag or its mutants in HeLa cells, extracts were incubated with anti-Flag Dynabeads, washed, and eluted as described above. For immunoprecipitation of LAMTOR1 in mouse hippocampus, extracts were incubated with anti-LAMTOR1 antibodies overnight and immunoprecipitates were collected with protein A/G Agarose. Proteins in inputs and precipitates were resolved by SDS-PAGE and analyzed by Western blotting, or analyzed using the Wes system as described below. All studies were performed in 3–5 independent experiments.

Wes protein analysis

The interaction between LAMTOR1 and TRPML1 *in vivo* was measured using a Wes automated capillary-based protein detection system (ProteinSimple) using 25-capillary 12- to 230-kDa Wes separation modules and anti-rabbit detection modules, according to the manufacturer's recommendations. Briefly, samples were diluted in a fluorescence-reducing buffer and heated to 95°C for 5 min before loading onto the Wes plate. A biotinylated ladder was included in all Wes experiments. Rows were successively loaded with antibody diluent, anti-TRPML1 (1:10, Alomone) or anti-LAMTOR1 (1:10, CST), horseradish peroxidase-conjugated anti-rabbit secondary antibody, and a luminol-peroxide mix. Data were analyzed using Compass for SW (ProteinSimple).

Intrahippocampal AAV injection

Stereotaxic AAV injection into CA1 region of the hippocampus was performed in 8-week-old mice. Under isoflurane anesthesia, LAMTOR1 or scrambled shRNA AAV in 1 µl solution were injected bilaterally into CA1 regions (coordinates: 2.00 mm posterior to bregma, 1.7 mm lateral to the midline and 1.4 mm below the dura). The solution was slowly injected over 10 min and the needle was left in place for an additional 5 min. The needle was then slowly withdrawn, and the incision closed. AAV-injected mice were used for experiments after four weeks.

Acute hippocampal slice preparation

Adult male mice (3-month-old) were anesthetized with gaseous isoflurane and decapitated. Brains were quickly removed and transferred to oxygenated, ice-cold cutting medium (in mM): 124 NaCl, 26 NaHCO₃, 10 glucose, 3 KCl, 1.25 KH₂PO₄, 5 MgSO₄, and 3.4 CaCl₂. Hippocampal transversal slices (400 µm-thick) were prepared using a McIlwain-type tissue chopper and (i) transferred to an interface recording chamber and exposed to a warm, humidified atmosphere of 95% O₂/5% CO₂ and continuously perfused with oxygenated and preheated (33 ± 0.5°C) artificial cerebrospinal fluid (aCSF) (in mM) [110 NaCl, 5 KCl, 2.5 CaCl₂, 1.5 MgSO₄, 1.24 KH₂PO₄, 10 D-glucose, 27.4 NaHCO₃], perfused at 1.4 ml/min

(electrophysiology); or (ii) cut under a fluorescence microscope to collect GFP-expressing CA1 areas and snap-frozen with dry ice (biochemical assays).

Electrophysiology

Electrophysiology was performed according to published protocols (Sun et al, 2018). After 1.5 h incubation at 33 ± 0.5°C in the recording chamber, a single glass pipette filled with 2 M NaCl was used to record field EPSPs (fEPSPs) elicited by stimulation of the Schaffer collateral pathway with twisted nichrome wires (single bare wire diameter, 50 µm) placed in CA1 stratum radiatum. Stimulation pulses were generated using a Multichannel Systems Model STG4002 Stimulator (Reutlingen, Germany). Responses were recorded through a differential amplifier (DAM 50, World Precision Instruments, USA) with a 10-kHz high-pass and 0.1-Hz low-pass filter. Before each experiment, the input/output (I/O) relation was examined by varying the intensity of the stimulation. Paired-pulse facilitation was tested at 20–300 ms interval. Long-term potentiation was induced using theta burst stimulation (10 bursts at 5 Hz, each burst consisting of 4 pulses at 100 Hz, with a pulse duration of 0.2 ms). Long-term depression was induced by 900 pulses delivered at 1 Hz. Data were collected and digitized by Clampex, and the slope of fEPSP was analyzed.

Immunofluorescence

For staining of LAMTOR1, LAMP2, GluA1, p-GluA1 S845, LAMTOR4, and mTOR, cultured hippocampal neurons were fixed in 2% paraformaldehyde (PFA)/10% sucrose for 15 min at 37°C, transferred to 0.05% Triton X-100/PBS for 5 min at 4°C, and then 0.02% Tween-20/PBS for 2 min at 4°C. Coverslips were washed twice with ice cold PBS and incubated 1 h in 3% BSA/PBS at room temperature. Cells were incubated with anti-LAMTOR1 (1:100, CST), anti-LAMP2 (1:200)/anti-GluA1 (1:100), anti-p-GluA1 S845 (1:100), anti-LAMTOR4 (1:500), and anti-LAMP2 (1:200)/anti-mTOR (1:100) respectively in 3% BSA/PBS overnight at 4°C. After three washes in PBS, cells were incubated with an appropriate Alexa Fluor-conjugated secondary antibody for 2 h at room temperature. Coverslips were then washed four times with PBS and mounted on glass slides using VECTASHIELD mounting medium with DAPI (Vector Laboratories). Images were acquired using a Zeiss LSM 880 confocal laser-scanning microscope in Airyscan mode. The staining was visualized in GFP-expressed neurons. For colocalization of GluA1 with LAMP2 analysis, neurons were preincubated with 200 µM leupeptin for 2.5 h before fixation to prevent GluA1 degradation (Goo et al, 2017). Colocalization of LAMP2 and GluA1 was then quantified manually with the following criteria. The two puncta were considered colocalized if GluA1 signal was either contained within the bounds of LAMP2 signal or overlapped it with more than 50% of the area inside the LAMP2 boundary. HeLa cells were stained as described above. The following primary antibodies were used: LAMTOR1 (1:100, CST), Flag (1:500, Sigma), and Flag (1:400, Abcam)/LAMP2 (1:50, Santa Cruz Biotechnology).

Hippocampal slices were collected 30 min after LFS and fixed in 4% PFA for 1 h and cryoprotected in 30% sucrose for 1 h at 4°C, and sectioned on a freezing microtome at 20 µm. Sections were blocked in 0.1 M of PBS containing 5% goat serum and 0.3% Triton X-100, and then incubated in primary antibody mixture including

chicken anti-GFP (1:500), rabbit anti-p-GluA1 S845 (1:100), and mouse anti-GluA1 (1:100) in 0.1 M PBS containing 1% BSA and 0.3% Triton X-100 overnight at 4°C. Sections were washed 3 times in PBS and incubated in Alexa Fluor 488 goat anti-chicken IgG, Alexa Fluor 594 goat anti-mouse IgG, and Alexa Fluor 633 goat anti-rabbit IgG for 2 h at room temperature. Separate staining of p-GluA1 and GluA1 was also performed by incubating slices in primary antibody mixture including chicken anti-GFP (1:500) and rabbit anti-p-GluA1 S845 (1:100) or rabbit anti-GluA1 (1:100). All images were taken in CA1 stratum radiatum between the stimulating and recording electrodes. GFP-expressing apical dendrites in hippocampal CA1 stratum radiatum were randomly selected for analysis. The threshold for the GFP fluorescence was set to make sure that the control slices from naive mice or mice with AAV infection but without GFP reporter were considered GFP-negative.

For immunofluorescence with brain tissue sections, deeply anesthetized animals were perfused, and brains were postfixed in 4% PFA overnight followed by sequential immersion in 15 and 30% sucrose for cryoprotection. Brains were then sectioned (20 µm) and stained as described above. The following primary antibodies were used: LAMTOR1 (1:200, Sigma) and GFP (1:500).

Proximity ligation assay (PLA)

Mice were injected with either control TAT or TAT-2031 as described above and perfused 2 h later. The Duolink PLA of brain tissue sections was performed according to the recommended protocol of the manufacturer with minor modifications. Permeabilized slices were mounted on glass slides, blocked, and incubated with rabbit anti-LAMTOR1 (1:200, sigma) and mouse anti-TRPML1 (1:10) (Thakore *et al*, 2020) overnight at 4°C. Negative controls were incubated with anti-LAMTOR1 only, anti-TRPML1 only, or omitting primary antibodies. Duolink PLA was then performed using anti-rabbit PLUS and anti-mouse MINUS PLA probes. Z-stack images were acquired at 1 µm intervals using a Zeiss LSM 880 confocal laser-scanning microscope in Airyscan mode and processed in Zen. The number of PLA signals was quantified using ImageJ.

Image analysis and quantification

Images for all groups in a particular experiment were obtained using identical acquisition parameters and analyzed using Zen (Zeiss) or ImageJ (NIH) software. In all cases, the experimenter was blind regarding the identity of the samples during acquisition and analysis. All immunostaining studies were performed in at least three independent experiments. Colocalization analysis by Mander's coefficients was performed using Zen unless otherwise indicated.

Novel object recognition

Novel object recognition was performed as previously described (Liu *et al*, 2016). Mice were randomly assigned to either control or LAMTOR1 shRNA groups and blinded to the examiner. Prior to training, mice habituated to the experimental apparatus for 5 min in the absence of objects. During habituation, animals were allowed to explore an empty arena. Twenty-four hours after habituation, animals were injected intraperitoneally (i.p.) with ML-SI1 (10 mg/kg body weight) 1 h before being exposed to the familiar arena with

two identical objects added and allowed to explore for 10 min. During the retention test 24 h later in which one object was replaced with a novel one, mice were allowed to explore the experimental apparatus for 6 min. Exploration was scored when a mouse's head was oriented toward the object within a distance of 1 cm or when the nose was touching the object. The relative exploration time (*t*) was recorded and expressed as a discrimination index (D.I. = $(t_{\text{novel}} - t_{\text{familiar}}) / (t_{\text{novel}} + t_{\text{familiar}}) \times 100\%$). Mean exploration times were then calculated and the discrimination indexes between groups compared. Mice that explored both objects for < 3 s in total during either training or testing were removed from further analysis. Mice that demonstrated an object preference during training (D.I. > ± 20) were also removed (Vogel-Ciernia *et al*, 2013).

Fear conditioning

Fear conditioning was performed as previously described (Sun *et al*, 2018). Four weeks after AAV injection, mice were injected intraperitoneally (i.p.) with ML-SI1 (10 mg/kg body weight) 1 h before being placed in the fear-conditioning chamber (H10-11M-TC, Coulbourn Instruments). The conditioning chamber was cleaned with 10% ethanol to provide a background odor. A ventilation fan provided a background noise at ~55 dB. After a 2-min exploration period, three tone-footshock pairings separated by 1-min intervals were delivered. The 85 dB 2 kHz tone lasted 30 s and coterminated with a footshock of 0.75 mA and 2 s. Mice remained in the training chamber for another 30 s before being returned to home cages. Context test was performed 1 day after training in the original conditioning chamber with 5-min recording. On day 3, animals were subjected to cue/tone test in a modified chamber with different texture and color, odor, background noise, and lighting. After 5-min recording, mice were exposed to a tone (85 dB, 2 kHz) for 1 min. Mouse behavior was recorded with the Freezeframe software and data were analyzed using the Freezeview software (Coulbourn Instruments). Motionless bouts lasting more than 1 s were considered as freezing. The percent of time animal froze was calculated.

Statistical analysis

All data are expressed as means ± SEM. To compute *P* values, unpaired Student's *t*-test, Mann-Whitney U test, one-way and two-way ANOVA with Tukey's, Dunnett's, or Sidak's post-test were used (GraphPad Prism 8), as indicated in figure legends. The level of statistical significance was set at *P* < 0.05. Additional information on statistics, including individual data points, tests, *P* values, and further statistical parameters, are provided in the Source Data.

Data availability

This study includes no data deposited in external repositories.

Expanded View for this article is available online.

Acknowledgements

This work was supported by grants MH101703 from NIMH to XB and NS104078 from NINDS to MB. XB is also supported by funds from the Daljit and Elaine Sarkaria Chair.

Author contributions

Jiandong Sun: Conceptualization; Data curation; Formal analysis; Supervision; Validation; Investigation; Visualization; Methodology; Writing—original draft; Writing—review & editing. **Yan Liu:** Data curation; Formal analysis; Investigation. **Xiaoning Hao:** Data curation; Validation; Investigation. **Weiju Lin:** Data curation; Formal analysis; Validation. **Wenyue Su:** Data curation; Formal analysis; Validation; Investigation. **Emerald Chiang:** Data curation; Validation; Investigation. **Michel Baudry:** Conceptualization; Supervision; Funding acquisition; Investigation; Writing—original draft; Project administration; Writing—review & editing. **Xiaoning Bi:** Conceptualization; Data curation; Supervision; Funding acquisition; Investigation; Visualization; Writing—original draft; Project administration; Writing—review & editing.

In addition to the CRediT author contributions listed above, the contributions in detail are:

JS, MB, and XB conceived and designed experiments and wrote the manuscript. JS and YL performed most of the experiments, analyzed data, and prepared the figures. XH and EC performed experiments. WL participated in data analysis. WS performed Wes protein analysis and real-time PCR analysis. MB and XB obtained funding and directed the research.

Disclosure and competing interests statement

The authors declare that they have no conflict of interest.

References

- Ambrosio AL, Boyle JA, Di Pietro SM (2015) TPC2 mediates new mechanisms of platelet dense granule membrane dynamics through regulation of Ca²⁺ release. *Mol Biol Cell* 26: 3263–3274
- Ayloo S, Guedes-Dias P, Ghiretti AE, Holzbaur ELF (2017) Dynein efficiently navigates the dendritic cytoskeleton to drive the retrograde trafficking of BDNF/TrkB signaling endosomes. *Mol Biol Cell* 28: 2543–2554
- Baas PW, Deitch JS, Black MM, Banker GA (1988) Polarity orientation of microtubules in hippocampal neurons: uniformity in the axon and nonuniformity in the dendrite. *Proc Natl Acad Sci U S A* 85: 8335–8339
- Bar-Peled L, Schweitzer LD, Zoncu R, Sabatini DM (2012) Ragulator is a GEF for the rag GTPases that signal amino acid levels to mTORC1. *Cell* 150: 1196–1208
- Baudry M, Bi X (2016) Calpain-1 and Calpain-2: the Yin and Yang of synaptic plasticity and neurodegeneration. *Trends Neurosci* 39: 235–245
- Baumgartel K, Mansuy IM (2012) Neural functions of calcineurin in synaptic plasticity and memory. *Learn Mem* 19: 375–384
- Beattie EC, Carroll RC, Yu X, Morishita W, Yasuda H, von Zastrow M, Malenka RC (2000) Regulation of AMPA receptor endocytosis by a signaling mechanism shared with LTD. *Nat Neurosci* 3: 1291–1300
- van Bommel B, Konietzny A, Kobler O, Bar J, Mikhaylova M (2019) F-actin patches associated with glutamatergic synapses control positioning of dendritic lysosomes. *EMBO J* 38: e101183
- Chakraborty K, Leung K, Krishnan Y (2017) High luminal chloride in the lysosome is critical for lysosome function. *eLife* 6: e28862
- Chazotte B (2011) Labeling Lysosomes in Live Cells with LysoTracker. *Cold Spring Harb Protoc* 2011: pdb.prot5571
- Chen T-W, Wardill TJ, Sun Yi, Pulver SR, Renninger SL, Baohan A, Schreiter ER, Kerr RA, Orger MB, Jayaraman V et al (2013) Ultrasensitive fluorescent proteins for imaging neuronal activity. *Nature* 499: 295–300
- Chu VT, Weber T, Wefers B, Wurst W, Sander S, Rajewsky K, Kuhn R (2015) Increasing the efficiency of homology-directed repair for CRISPR-Cas9-induced precise gene editing in mammalian cells. *Nat Biotechnol* 33: 543–548
- Davis LC, Morgan AJ, Galione A (2020) NAADP-regulated two-pore channels drive phagocytosis through endo-lysosomal Ca²⁺ nanodomains, calcineurin and dynamin. *EMBO J* 39: e104058
- de Araujo MEG, Naschberger A, Fürnrohr BG, Stasyk T, Dunzendorfer-Matt T, Lechner S, Welti S, Kremser L, Shivalingaiah G, Offterdinger M et al (2017) Crystal structure of the human lysosomal mTORC1 scaffold complex and its impact on signaling. *Science* 358: 377–381
- Dong X-P, Shen D, Wang X, Dawson T, Li X, Zhang QI, Cheng X, Zhang Y, Weisman LS, Delling M et al (2010) PI(3,5)P(2) controls membrane trafficking by direct activation of mucolipin Ca²⁺ release channels in the endolysosome. *Nat Commun* 1: 38
- Dudek SM, Bear MF (1993) Bidirectional long-term modification of synaptic effectiveness in the adult and immature hippocampus. *J Neurosci* 13: 2910–2918
- Eskelinen EL (2006) Roles of LAMP-1 and LAMP-2 in lysosome biogenesis and autophagy. *Mol Aspects Med* 27: 495–502
- Farfel-Becker T, Roney JC, Cheng XT, Li S, Cuddy SR, Sheng ZH (2019) Neuronal soma-derived degradative lysosomes are continuously delivered to distal axons to maintain local degradation capacity. *Cell Rep* 28: 51–64.e4
- Farias GG, Guardia CM, De Pace R, Britt DJ, Bonifacino JS (2017) BORC/kinesin-1 ensemble drives polarized transport of lysosomes into the axon. *Proc Natl Acad Sci U S A* 114: E2955–E2964
- Fernandez-Monreal M, Brown TC, Royo M, Esteban JA (2012) The balance between receptor recycling and trafficking toward lysosomes determines synaptic strength during long-term depression. *J Neurosci* 32: 13200–13205
- Filipek PA, de Araujo MEG, Vogel GF, De Smet CH, Eberharter D, Rebsamen M, Rudashevskaya EL, Kremser L, Yordanov T, Tschakner P et al (2017) LAMTOR/Ragulator is a negative regulator of Arl8b- and BORC-dependent late endosomal positioning. *J Cell Biol* 216: 4199–4215
- Firestone AJ, Weinger JS, Maldonado M, Barlan K, Langston LD, O'Donnell M, Gelfand VI, Kapoor TM, Chen JK (2012) Small-molecule inhibitors of the AAA+ ATPase motor cytoplasmic dynein. *Nature* 484: 125–129
- Garrity AG, Wang W, Collier CM, Levey SA, Gao Q, Xu H (2016) The endoplasmic reticulum, not the pH gradient, drives calcium refilling of lysosomes. *eLife* 5: e15887
- Goo MS, Sancho L, Slepak N, Boassa D, Deerinck TJ, Ellisman MH, Bloodgood BL, Patrick GN (2017) Activity-dependent trafficking of lysosomes in dendrites and dendritic spines. *J Cell Biol* 216: 2499–2513
- Guo M, Lu Y, Garza JC, Li Y, Chua SC, Zhang W, Lu B, Lu XY (2012) Forebrain glutamatergic neurons mediate leptin action on depression-like behaviors and synaptic depression. *Transl Psychiatry* 2: e83
- Hata M, Ikeda HO, Iwai S, Iida Y, Gotoh N, Asaka I, Ikeda K, Isobe Y, Hori A, Nakagawa S et al (2018) Reduction of lipid accumulation rescues Bietti's crystalline dystrophy phenotypes. *Proc Natl Acad Sci U S A* 115: 3936–3941
- Hay N, Sonenberg N (2004) Upstream and downstream of mTOR. *Genes Dev* 18: 1926–1945
- Jongsma M, Berlin I, Wijdeven R, Janssen L, Janssen G, Garstka M, Janssen H, Mensink M, van Veelen P, Spaapen R et al (2016) An ER-associated pathway defines endosomal architecture for controlled cargo transport. *Cell* 166: 152–166
- Kapitein LC, Schlager MA, Kuijpers M, Wulf PS, van Spronsen M, MacKintosh FC, Hoogenraad CC (2010) Mixed microtubules steer dynein-driven cargo transport into dendrites. *Curr Biol* 20: 290–299

- Li X, Rydzewski N, Hider A, Zhang X, Yang J, Wang W, Gao Q, Cheng X, Xu H (2016) A molecular mechanism to regulate lysosome motility for lysosome positioning and tubulation. *Nat Cell Biol* 18: 404–417
- Liu Y, Sun J, Wang Y, Lopez D, Tran J, Bi X, Baudry M (2016) Deleting both PHLPP1 and CANP1 rescues impairments in long-term potentiation and learning in both single knockout mice. *Learn Mem* 23: 399–404
- Malenka RC, Bear MF (2004) LTP and LTD: an embarrassment of riches. *Neuron* 44: 5–21
- Man HY, Sekine-Aizawa Y, Hugarir RL (2007) Regulation of α -amino-3-hydroxy-5-methyl-4-isoxazolepropionic acid receptor trafficking through PKA phosphorylation of the Glu receptor 1 subunit. *Proc Natl Acad Sci U S A* 104: 3579–3584
- Mangeol P, Prevo B, Peterman EJ (2016) KymographClear and KymographDirect: two tools for the automated quantitative analysis of molecular and cellular dynamics using kymographs. *Mol Biol Cell* 27: 1948–1957
- Mayle KM, Le AM, Kamei DT (2012) The intracellular trafficking pathway of transferrin. *Biochim Biophys Acta* 1820: 264–281
- Medina DL, Di Paola S, Peluso I, Armani A, De Stefani D, Venditti R, Montefusco S, Scotto-Rosato A, Prezioso C, Forrester A et al (2015) Lysosomal calcium signalling regulates autophagy through calcineurin and TFEB. *Nat Cell Biol* 17: 288–299
- Medina D, Fraldi A, Bouche V, Annunziata F, Mansueto G, Spampanato C, Puri C, Pignata A, Martina J, Sardiello M et al (2011) Transcriptional activation of lysosomal exocytosis promotes cellular clearance. *Dev Cell* 21: 421–430
- Minichiello L (2009) TrkB signalling pathways in LTP and learning. *Nat Rev Neurosci* 10: 850–860
- Misko A, Wood L, Kiselyov K, Slaugenhaupt S, Grishchuk Y (2021) Progress in elucidating pathophysiology of mucopolipidosis IV. *Neurosci Lett* 755: 135944
- Morgan AJ, Platt FM, Lloyd-Evans E, Galione A (2011) Molecular mechanisms of endolysosomal Ca^{2+} signalling in health and disease. *Biochem J* 439: 349–374
- Mulkey RM, Endo S, Shenolikar S, Malenka RC (1994) Involvement of a calcineurin/inhibitor-1 phosphatase cascade in hippocampal long-term depression. *Nature* 369: 486–488
- Nada S, Hondo A, Kasai A, Koike M, Saito K, Uchiyama Y, Okada M (2009) The novel lipid raft adaptor p18 controls endosome dynamics by anchoring the MEK-ERK pathway to late endosomes. *EMBO J* 28: 477–489
- Nakahata Y, Yasuda R (2018) Plasticity of spine structure: local signaling, translation and cytoskeletal reorganization. *Front Synaptic Neurosci* 10: 29
- Nicoll RA (2017) A brief history of long-term potentiation. *Neuron* 93: 281–290
- Onyenwoke RU, Sexton JZ, Yan F, Diaz MC, Forsberg LJ, Major MB, Brenman JE (2015) The mucopolipidosis IV Ca^{2+} channel TRPML1 (MCOLN1) is regulated by the TOR kinase. *Biochem J* 470: 331–342
- Padamsey Z, McGuinness L, Bardo SJ, Reinhart M, Tong R, Hedegaard A, Hart ML, Emptage NJ (2017) Activity-dependent exocytosis of lysosomes regulates the structural plasticity of dendritic spines. *Neuron* 93: 132–146
- Park S, Ahuja M, Kim MS, Brailoiu GC, Jha A, Zeng M, Baydyuk M, Wu LG, Wassif CA, Porter FD et al (2016) Fusion of lysosomes with secretory organelles leads to uncontrolled exocytosis in the lysosomal storage disease mucopolipidosis type IV. *EMBO Rep* 17: 266–278
- Patterson M, Yasuda R (2011) Signalling pathways underlying structural plasticity of dendritic spines. *Br J Pharmacol* 163: 1626–1638
- Pinar C, Fontaine CJ, Trivino-Paredes J, Lottenberg CP, Gil-Mohapel J, Christie BR (2017) Revisiting the flip side: long-term depression of synaptic efficacy in the hippocampus. *Neurosci Biobehav Rev* 80: 394–413
- Pu J, Keren-Kaplan T, Bonifacino JS (2017) A regulator-BORC interaction controls lysosome positioning in response to amino acid availability. *J Cell Biol* 216: 4183–4197
- Ran FA, Hsu PD, Wright J, Agarwala V, Scott DA, Zhang F (2013) Genome engineering using the CRISPR-Cas9 system. *Nat Protoc* 8: 2281–2308
- Raychowdhury MK, Gonzalez-Perrett S, Montalbetti N, Timpanaro GA, Chasan B, Goldmann WH, Stahl S, Cooney A, Goldin E, Cantiello HF (2004) Molecular pathophysiology of mucopolipidosis type IV: pH dysregulation of the mucolipin-1 cation channel. *Hum Mol Genet* 13: 617–627
- Samie M, Wang X, Zhang X, Goschka A, Li X, Cheng X, Gregg E, Azar M, Zhuo Y, Garrity A et al (2013) A TRP channel in the lysosome regulates large particle phagocytosis via focal exocytosis. *Dev Cell* 26: 511–524
- Sancak Y, Bar-Peled L, Zoncu R, Markhard AL, Nada S, Sabatini DM (2010) Ragulator-Rag complex targets mTORC1 to the lysosomal surface and is necessary for its activation by amino acids. *Cell* 141: 290–303
- Santoni G, Maggi F, Amantini C, Marinelli O, Nabissi M, Morelli MB (2020) Pathophysiological role of transient receptor potential mucolipin channel 1 in calcium-mediated stress-induced neurodegenerative diseases. *Front Physiol* 11: 251
- Scheffler JM, Sparber F, Tripp CH, Herrmann C, Humenberger A, Blitz J, Romani N, Stoitzner P, Huber LA (2014) LAMTOR2 regulates dendritic cell homeostasis through FLT3-dependent mTOR signalling. *Nat Commun* 5: 5138
- Shen D, Wang X, Li X, Zhang X, Yao Z, Dibble S, Dong X-P, Yu T, Lieberman AP, Showalter HD et al (2012) Lipid storage disorders block lysosomal trafficking by inhibiting a TRP channel and lysosomal calcium release. *Nat Commun* 3: 731
- Sherer NM, Lehmann MJ, Jimenez-Soto LF, Ingmundson A, Horner SM, Cicchetti G, Allen PG, Pypaert M, Cunningham JM, Mothes W (2003) Visualization of retroviral replication in living cells reveals budding into multivesicular bodies. *Traffic* 4: 785–801
- Shi M, Chen B, Mahajan D, Boh BK, Zhou Y, Dutta B, Tie HC, Sze SK, Wu G, Lu L (2018) Amino acids stimulate the endosome-to-Golgi trafficking through Ragulator and small GTPase Arl5. *Nat Commun* 9: 4987
- Sun J, Liu Y, Jia Y, Hao X, Lin WJ, Tran J, Lynch G, Baudry M, Bi X (2018) UBE3A-mediated p18/LAMTOR1 ubiquitination and degradation regulate mTORC1 activity and synaptic plasticity. *eLife* 7: e37993
- Sun J, Zhu G, Liu Y, Standley S, Ji A, Tunuguntla R, Wang Y, Claus C, Luo Y, Baudry M et al (2015) UBE3A regulates synaptic plasticity and learning and memory by controlling SK2 channel endocytosis. *Cell Rep* 12: 449–461
- Tas RP, Chazeau A, Cloin BMC, Lambers MLA, Hoogenraad CC, Kapitein LC (2017) Differentiation between oppositely oriented microtubules controls polarized neuronal transport. *Neuron* 96: 1264–1271.e5
- Thakore P, Pritchard HAT, Griffin CS, Yamasaki E, Drumm BT, Lane C, Sanders KM, Feng Earley Y, Earley S (2020) TRPML1 channels initiate Ca^{2+} sparks in vascular smooth muscle cells. *Sci Signal* 13: eaba1015
- Venkatachalam K, Hofmann T, Montell C (2006) Lysosomal localization of TRPML3 depends on TRPML2 and the mucopolipidosis-associated protein TRPML1. *J Biol Chem* 281: 17517–17527
- Vogel-Ciernia A, Matheos D, Barrett R, Wood MA (2013) The neuron-specific chromatin regulatory subunit BAF53b is necessary for epigenetic regulation of synaptic plasticity and memory. *Neuropsychopharmacology* 38: S325–S326
- Wagner JJ, Alger BE (1995) GABAergic and developmental influences on homosynaptic LTD and depotentiation in rat hippocampus. *J Neurosci* 15: 1577–1586

- Wagner SA, Beli P, Weinert BT, Nielsen ML, Cox J, Mann M, Choudhary C (2011) A proteome-wide, quantitative survey of *in vivo* ubiquitylation sites reveals widespread regulatory roles. *Mol Cell Proteomics* 10: M111.013284
- Xu H, Ren D (2015) Lysosomal physiology. *Annu Rev Physiol* 77: 57–80
- Yap CC, Digilio L, McMahon LP, Garcia ADR, Winckler B (2018) Degradation of dendritic cargos requires Rab7-dependent transport to somatic lysosomes. *J Cell Biol* 217: 3141–3159
- Yonehara R, Nada S, Nakai T, Nakai M, Kitamura A, Ogawa A, Nakatsumi H, Nakayama KI, Li S, Standley DM et al (2017) Structural basis for the assembly of the Ragulator-Rag GTPase complex. *Nat Commun* 8: 1625
- Zhang C-S, Jiang B, Li M, Zhu M, Peng Y, Zhang Y-L, Wu Y-Q, Li T, Liang YU, Lu Z et al (2014) The lysosomal v-ATPase-Ragulator complex is a common activator for AMPK and mTORC1, acting as a switch between catabolism and anabolism. *Cell Metab* 20: 526–540
- Zhang X, Li X, Xu H (2012) Phosphoinositide isoforms determine compartment-specific ion channel activity. *Proc Natl Acad Sci U S A* 109: 11384–11389



License: This is an open access article under the terms of the Creative Commons Attribution-NonCommercial-NoDerivs License, which permits use and distribution in any medium, provided the original work is properly cited, the use is non-commercial and no modifications or adaptations are made.